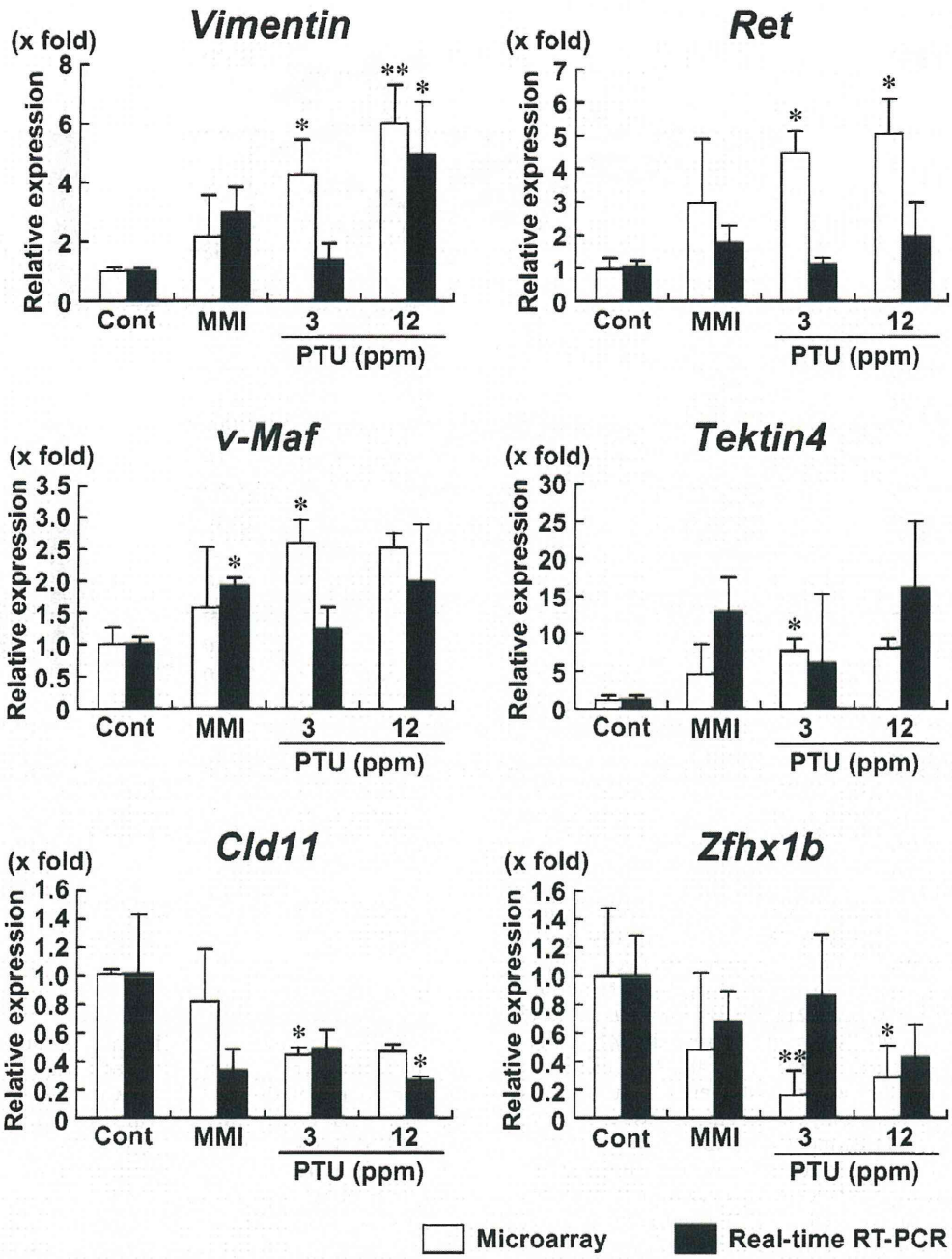

Fig. 3. Validation of mRNA expression of genes selected from microarray data ($n = 4$ in each group). *$P < 0.05$, **$P < 0.01$ vs. untreated controls.

up- or down-regulation in response to 200 ppm MMI was much lower compared with those of both PTU groups. Four hundred and eighty six common genes (428 up-regulated; 58 down-regulated) were identified with altered expression between MMI and both PTU groups (Fig. 2 and Supplementary data: Tables 1 and 2). Among these genes, the genes associated with central nervous system (CNS) development, cell differentiation and cell adhesion were commonly up- or down-regulated in response to anti-thyroid agents (Supplementary data: Tables 1 and 2). Twenty-four genes (20 up-regulated; 4 down-regulated) were related to CNS development involving glial cell differentiation, axon guidance, myelination, and cellular migration (Table 1). Among them, 12 up-regulated genes and two down-regulated genes showed PTU dose-dependent expression changes. For confirmation of microarray data, four genes that were up-regulated and two genes that were down-regulated in response to anti-thyroid agents were selected for mRNA expression analysis by real-time RT-PCR. Results are summarized in Fig. 3. All genes examined showed fluctuations in transcript levels in any of anti-thyroid agent treatment groups, which was similar to that of microarray data.

3.2. *Immunolocalization of selected molecules in cerebral white matter*

Immunohistochemical localization of vimentin, Ret, DCC and Cld11 was examined in the cerebral white matter. Within white

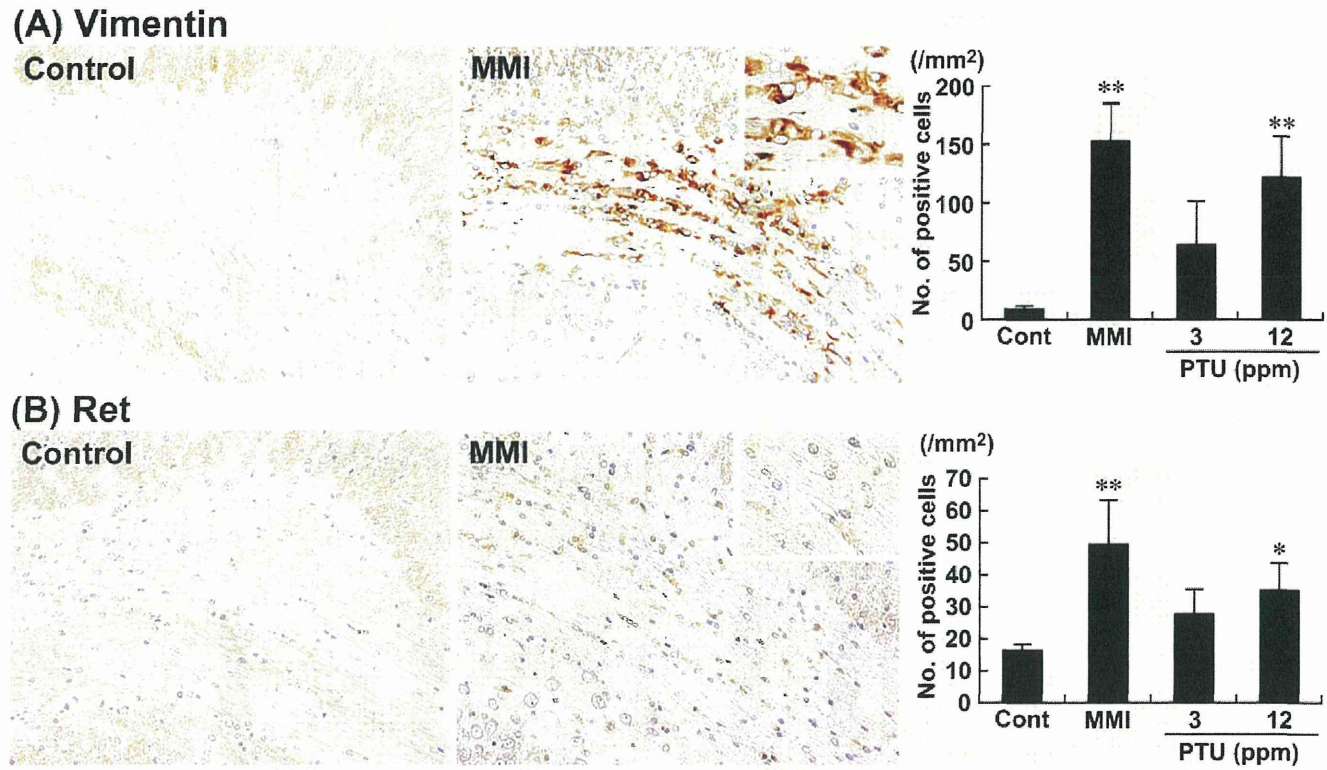

Fig. 4. Immunohistochemical distributions of vimentin- and Ret-positive cells in the while matter tissue. (A) Vimentin-immunoreactive cells in the cingulum. Untreated control animal (left) and MMI-treated animal (right). 200× magnification (inset: 400× magnification). Graph shows the mean number of positive cells within the cingulum at 200× magnification (untreated controls: $n=6$; MMI and PTU groups: $n=10$). $^{**}P<0.01$ vs. untreated controls. (B) Ret-immunoreactive cells in the cingulum. Untreated control animal (left), MMI-treated animal (right). 200× magnification (inset: 400× magnification). Graph shows the mean number of positive cells within the cingulum at 100× magnification (untreated controls: $n=6$; MMI and PTU groups: $n=10$). $^{*}P<0.05$, $^{**}P<0.01$ vs. untreated controls.

matter tissues, vimentin-immunoreactive cells were scarcely distributed in untreated control animals (Fig. 4A). After treatment with anti-thyroid agents, the distribution of vimentin-positive cells were mainly observed in the cingulum with a statistically significant increase in number with MMI and 12 ppm PTU treatments (Fig. 4A).

Ret-immunoreactive cells were mainly observed in white matter tissues of untreated control animals (Fig. 4B). After treatment with anti-thyroid agents, Ret-positive cells were mainly observed in the cingulum with a statistically significant increase in number with MMI and 12 ppm PTU treatments (Fig. 4B).

DCC showed diffuse immunoreactivity in white matter, indicating myelin sheaths with a statistically significant increase in the intensity scores of animals treated with MMI and 12 ppm PTU as compared with those of the untreated control (Fig. 5A).

Diffuse Cld11-immunoreactivity was observed in white matter, indicating myelin sheaths (Fig. 5B). The immunoreactivity showed a statistically significant increase in the intensity score of animals treated with MMI as compared with that of the untreated control (Fig. 5B).

3.3. Immunolocalization of GFAP

To investigate the cell type of vimentin-positive cells, cellular distribution of GFAP immunoreactivity was analyzed as a marker of astrocytes. Untreated control animals showed scattered distribution of GFAP-immunoreactive cells in cerebral white matter, and the number of GFAP-immunoreactive cells was higher compared with that of vimentin-positive cells. GFAP-immunoreactive cells showed a similar distribution to that of vimentin-immunoreactive cells, with accumulated distribution in the cingulum (Fig. 6). After treatment with anti-thyroid agents, the number of GFAP-positive cells was significantly increased in animals treated with MMI and 12 ppm PTU.

4. Discussion

In our previous study [16], maternal exposure to MMI and PTU induced typical hypothyroidism-related changes in the concentration of thyroid-related hormones, and variability in the distribution of hippocampal CA1 pyramidal neurons due to neuronal mismigration [16]. With regard to thyroid hormone-related changes in functions or structures in glial cell populations, gene expression alternations have been reported in myelin-related protein genes related to oligodendrocytes [20,21], as well as in enzymes or cytoskeletal components related to astrocytes [22–24]. Therefore, both oligodendrocytes and astrocytes could also be the target of developmental hypothyroidism. We, in the above-mentioned study [16], also observed changes in white matter structures with hypoplasia due to impaired oligodendroglial development as previously reported [2,9]. Using the same study samples, we, in the present study, analyzed immunohistochemical distribution of molecules that showed fluctuations in gene expression from microarray analysis of cerebral white matter tissue collected using microdissection targeting oligodendrocytes and astrocytes. This is the first report to use microarray analysis of gene expression changes induced by developmental hypothyroidism in white matter, whereas there have been such approaches for the study of cerebral cortex and hippocampal substructures [15,25,26]. We found that anti-thyroid agents caused fluctuations in a number of genes associated with CNS development involving glial cell differentiation, axon guidance, myelination, and cellular migration as listed in Table 1. Among them, vimentin, Ret, DCC and Cld11

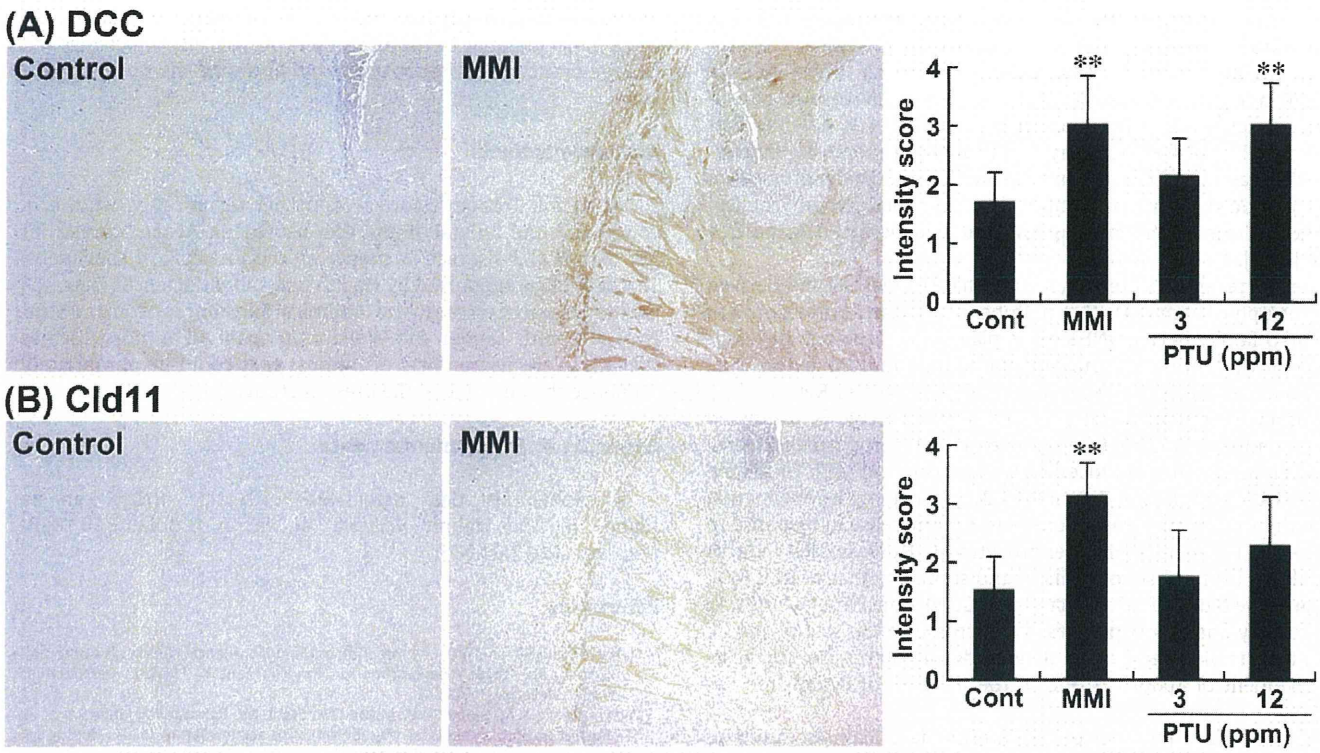

Fig. 5. Immunohistochemical distributions of DCC- and Cld11 in the while matter tissue. (A) DCC-immunoreactivity in the myelin sheath of the external capsule, internal capsule, and fimbria of the hippocampus. Untreated control animal (left), MMI-treated animal (right). 40× magnification. Graph shows the mean intensity score of immunoreactivity at 40× magnification (untreated controls: $n = 6$; MMI and PTU groups: $n = 10$). $^{**}P < 0.01$ vs. untreated controls. (B) Cld11-immunoreactivity in the myelin sheath of the external capsule, internal capsule, and fimbria of the hippocampus. Untreated control animal (left), MMI-treated animal (right). 40× magnification. Graph shows the mean intensity score of immunoreactivity at 40× magnification (untreated controls: $n = 6$; MMI and PTU groups: $n = 10$). $^{**}P < 0.01$ vs. untreated controls.

showed immunohistochemical distribution changes in the cerebral white matter of offspring after maternal exposure to PTU and MMI.

Cld11 is a four-transmembrane protein, which is primarily expressed in oligodendrocytes of the CNS and is the third most abundant CNS myelin protein [27–29]. Cld11 is involved in the formation of intramembranous tight junctions within the myelin sheath [30]. It is known that developmental hypothyroidism results in continued reduction of oligodendrocytes in the CC region from PND 10 [2]. In vitro study has shown that Cld11-overexpression results in induction of oligodendrocyte proliferation [31]. This result indicates that the overexpression of Cld11 at PND 20 is a compensatory response to decrease numbers of oligodendrocytes. However, mRNA levels were inconsistently decreased, suggesting involvement of post-transcriptional events such as those regulating mRNA stability and protein turnover.

DCC is a transmembrane receptor for netrin-1 via the fourth fibronectin type III domain [32]. Netrin-1 is a secreted protein, which elicits both attractive and repulsive responses in axonal guidance, neuronal migration and oligodendroglial migration depending on the homomeric or heteromeric combination of receptor dimers including DCC and Unc5 [33–35]. Netrin-1 signaling via DCC mediates growth cone extension and myelin sheath formation [36,37]. Therefore, increased expression of DCC in the myelin sheath at PND 20 induced by developmental hypothyroidism in the present study suggests a compensatory increase in response to suppression of myelin sheath formation [2]. However,

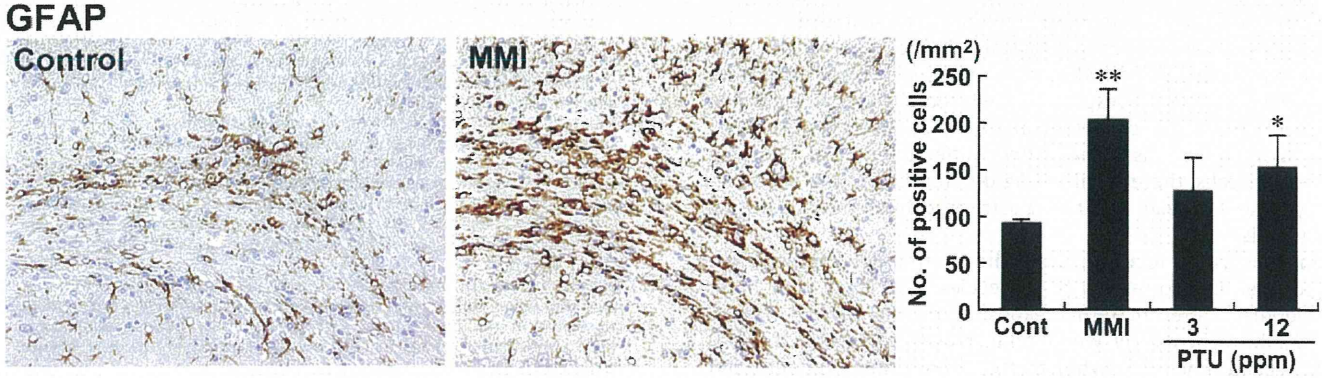

Fig. 6. Immunohistochemical distributions of GFAP-positive cells in the cingulum. Untreated control animal (left), MMI-treated animal (right). 200× magnification. Graph shows the mean number of positive cells within the cingulum at 200× magnification (untreated controls: $n = 6$; MMI and PTU groups: $n = 10$). $^{*}P < 0.05$, $^{**}P < 0.01$ vs. untreated controls.

DCC has an alternative function to drive cell death independent of both mitochondria-dependent and death receptor/caspase-8 pathways [38,39]. Moreover, DCC induces cell death in the absence of netrin-1 [40]. Because we did not find an increase in netrin-1 transcript levels using microarray analysis, it is possible that increased ligand-free DCC may lead to glial cell apoptosis. Progressive decrease in the CC area and the number of oligodendrocytes in this area during maturation after developmental hypothyroidism suggests the involvement of apoptosis due to increased ligand-free DCC [2,16].

Ret is a receptor protein–tyrosine kinase of glial cell line-derived neurotrophic factor (GDNF), a member of the transforming growth factor-β family [41]. GDNF signals play a critical role in development of the entire nervous system, kidney morphogenesis and spermatogenesis. While the functional relevance of Ret in oligodendrocytes has not been reported, this molecule is expressed in progenitor and immature oligodendrocytes in vitro and mediates cell proliferation induced by GDNF treatment [42]. Therefore, increased expression of Ret on PND 20 proceeding developmental hypothyroidism suggests a compensatory increase in response to decreased numbers of oligodendrocytes [2]. However, Ret induces cell death in the absence of its ligand similar to that of DCC [43]. Because we did not find an increase in GDNF transcript levels using microarray analysis, a progressive decrease in the size of the CC area and its oligodendrocyte density during maturation suggests involvement of apoptosis due to the increase of ligand-free Ret [2,16].

Vimentin is a member of the intermediate filament family of proteins. In the brain, this molecule is expressed in immature astrocytes during development [44–46]. Reactive astrocytes that are activated immature astrocytes during gliosis processes in response to injuries of CNS tissue also express vimentin [47,48]. Reactive astrocytes also express GFAP similar to that of mature astrocytes [47,48], suggesting that immature astrocytes can express both of vimentin and GFAP. On the other hand, developmental hypothyroidism leads to increase in vimentin expression in fetal rat brains [23]. Increase of GFAP-expression was also reported after developmental hypothyroidism in the CC region on PND 15 [49]. These results may suggest that developmental hypothyroidism increases the immature population of astrocytes. In the present study, vimentin-immunoreactive cells showed similar localization to those positive for GFAP. Therefore, a larger population of vimentin-positive cells in the cingulum induced by developmental hypothyroidism was considered to consist of immature astrocytes resembling reactive astrocytes. Interestingly, we previously reported frequent induction of subcortical band heterotopia in the CC, manifested by the appearance of aberrant cortical tissue in this anatomical area, in hypothyroid animals identical to the present study [16]. Anatomical location of this heterotopic tissue was close to the cingulum accumulating immature astrocytes, suggesting an etiological relation between the two. Alternatively, the increased immature astrocytes may simply be the reactive change in response to reduced oligodendrocytes due to developmental hypothyroidism [2,16,49]. However, developmental hypothyroidism may affect differentiation of neuronal progenitor cells, thereby inhibiting differentiation into oligodendrocytes, and instead, facilitating astrocytic differentiation during gliogenesis.

In conclusion, focusing on white matter development, we found aberrant expression of molecules associated with brain development after maternal exposure to anti-thyroid agents. Immunohistochemically, we found increased expression of Cld11, DCC, Ret and vimentin in white matter. Among them, vimentin and Ret were expressed in immature astrocytes and oligodendrocytes, respectively. Both positive cell populations were mainly distributed in the cingulum with the largest area of white matter. Because vimentin- and Ret-positive cells can be quantitatively evaluated, these molecules may be useful markers of glial cells, which respond to developmental exposure to thyroid hormone-disrupting chemicals.

Acknowledgments

We thank Tomomi Morikawa for her technical assistance in conducting the animal study. We also thank Ayako Kaneko for her technical assistance in preparing the histological specimens. This work was supported by Health and Labour Sciences Research Grants (Research on the Risk of Chemical Substances) from the Ministry of Health, Labour and Welfare of Japan. All authors disclose that there are no conflicts of interest that could inappropriately influence the outcome of the present study.

Appendix A. Supplementary data

Supplementary data associated with this article can be found, in the online version, at http://dx.doi.org/10.1016/j.reprotox.2012.03.005.

References

[1] Porterfield SP. Thyroidal dysfunction and environmental chemicals—potential impact on brain development. Environmental Health Perspectives 2000;108(Suppl. 3):433–8.
[2] Schoonover CM, Seibel MM, Jolson DM, Stack MJ, Rahman RJ, Jones SA, et al. Thyroid hormone regulates oligodendrocyte accumulation in developing rat brain white matter tracts. Endocrinology 2004;145:5013–20.
[3] Montero-Pedrazuela A, Venero C, Lavado-Autric R, Fernández-Lamo I, García-Verdugo JM, Bernal J, et al. Modulation of adult hippocampal neurogenesis by thyroid hormones: implications in depressive-like behavior. Molecular Psychiatry 2006;11:361–71.
[4] de Escobar GM, Obregón MJ, del Rey FE. Iodine deficiency and brain development in the first half of pregnancy. Public Health Nutrition 2007;10:1554–70.
[5] Comer CP, Norton S. Effects of perinatal methimazole exposure on a developmental test battery for neurobehavioral toxicity in rats. Toxicology and Applied Pharmacology 1982;63:133–41.
[6] Akaike M, Kato N, Ohno H, Kobayashi T. Hyperactivity and spatial maze learning impairment of adult rats with temporary neonatal hypothyroidism. Neurotoxicology and Teratology 1991;13:317–22.
[7] Guadaño Ferraz A, Escobar del Rey F, Morreale de Escobar G, Innocenti GM, Berbel P. The development of the anterior commissure in normal and hypothyroid rats. Brain Research Developmental Brain Research 1994;81:293–308.
[8] Lavado-Autric R, Ausó E, García-Velasco JV, Arufe Mdel C, Escobar del Rey F, Berbel P, et al. Early maternal hypothyroxinemia alters histogenesis and cerebral cortex cytoarchitecture of the progeny. Journal of Clinical Investigation 2003;111:954–7.
[9] Goodman JH, Gilbert ME. Modest thyroid hormone insufficiency during development induces a cellular malformation in the corpus callosum: a model of cortical dysplasia. Endocrinology 2007;148:2593–7.
[10] Shibutani M, Uneyama C, Miyazaki K, Toyoda K, Hirose M. Methacarn fixation: a novel tool for analysis of gene expressions in paraffin-embedded tissue specimens. Laboratory Investigation 2000;80:199–208.
[11] Uneyama C, Shibutani M, Masutomi N, Takagi H, Hirose M. Methacarn fixation for genomic DNA analysis in microdissected, paraffin-embedded tissue specimens. Journal of Histochemistry and Cytochemistry 2002;50:1237–45.
[12] Takagi H, Shibutani M, Kato N, Fujita H, Lee KY, Takigami S, et al. Microdissected region-specific gene expression analysis with methacarn-fixed, paraffin-embedded tissues by real-time RT-PCR. Journal of Histochemistry and Cytochemistry 2004;52:903–13.
[13] Shibutani M, Lee KY, Igarashi K, Woo GH, Inoue K, Nishimura T, et al. Hypothalamus region-specific global gene expression profiling in early stages of central endocrine disruption in rat neonates injected with estradiol benzoate or flutamide. Developmental Neurobiology 2007;67:253–69.
[14] Woo GH, Takahashi M, Inoue K, Fujimoto H, Igarashi K, Kanno J, et al. Cellular distributions of molecules with altered expression specific to thyroid proliferative lesions developing in a rat thyroid carcinogenesis model. Cancer Science 2009;100:617–25.
[15] Saegusa Y, Woo GH, Fujimoto H, Inoue K, Takahashi M, Hirose M, et al. Gene expression profiling and cellular distribution of molecules with altered expression in the hippocampal CA1 region after developmental exposure to anti-thyroid agents in rats. Journal of Veterinary Medical Science 2010;72:187–95.
[16] Shibutani M, Woo GH, Fujimoto H, Saegusa Y, Takahashi M, Inoue K, et al. Assessment of developmental effects of hypothyroidism in rats from in utero and lactation exposure to anti-thyroid agents. Reproductive Toxicology 2009;28:297–307.

[17] Masutomi N, Shibutani M, Takagi H, Uneyama C, Takahashi N, Hirose M. Impact of dietary exposure to methoxychlor, genistein, or diisononyl phthalate during the perinatal period on the development of the rat endocrine/reproductive systems in later life. Toxicology 2003;192:149–70.
[18] Nakamura R, Teshima R, Hachisuka A, Sato Y, Takagi K, Nakamura R, et al. Effects of developmental hypothyroidism induced by maternal administration of methimazole or propylthiouracil on the immune system of rats. International Immunopharmacology 2007;7:1630–8.
[19] Lee KY, Shibutani M, Inoue K, Kuroiwa K, U M, Woo GH, et al. Methacarn fixation—effects of tissue processing and storage conditions on detection of mRNAs and proteins in paraffin-embedded tissues. Analytical Biochemistry 2006;351:36–43.
[20] Ibarrola N, Rodríguez-Peña A. Hypothyroidism coordinately and transiently affects myelin protein gene expression in most rat brain regions during postnatal development. Brain Research 1997;752:285–93.
[21] Barradas PC, Vieira RS, De Freitas MS. Selective effect of hypothyroidism on expression of myelin markers during development. Journal of Neuroscience Research 2001;66:254–61.
[22] Farwell AP, Dubord-Tomasetti SA. Thyroid hormone regulates the expression of laminin in the developing rat cerebellum. Endocrinology 1999;140:4221–7.
[23] Evans IM, Pickard MR, Sinha AK, Leonard AJ, Sampson DC, Ekins RP. Influence of maternal hyperthyroidism in the rat on the expression of neuronal and astrocytic cytoskeletal proteins in fetal brain. Journal of Endocrinology 2002;175:597–604.
[24] Dasgupta A, Das S, Sarkar PK. Thyroid hormone promotes glutathione synthesis in astrocytes by up regulation of glutamate cysteine ligase through differential stimulation of its catalytic and modulator subunit mRNAs. Free Radical Biology and Medicine 2007;42:617–26.
[25] Royland JE, Parker JS, Gilbert ME. A genomic analysis of subclinical hypothyroidism in hippocampus and neocortex of the developing rat brain. Journal of Neuroendocrinology 2008;20:1319–38.
[26] Kobayashi K, Akune H, Sumida K, Saito K, Yoshioka T, Tsuji R. Perinatal exposure to PTU decreases expression of Arc, Homer 1, Egr 1 and Kcna 1 in the rat cerebral cortex and hippocampus. Brain Research 2009;1264:24–32.
[27] Bronstein JM, Popper P, Micevych PE, Farber DB. Isolation and characterization of a novel oligodendrocyte-specific protein. Neurology 1996;47:772–8.
[28] Bronstein JM, Micevych PE, Chen K. Oligodendrocyte-specific protein (OSP) is a major component of CNS myelin. Journal of Neuroscience Research 1997;50:713–20.
[29] Morita K, Sasaki H, Fujimoto K, Furuse M, Tsukita S. Claudin-11/OSP-based tight junctions of myelin sheaths in brain and Sertoli cells in testis. Journal of Cell Biology 1999;145:579–88.
[30] Gow A, Southwood CM, Li JS, Pariali M, Riordan GP, Brodie SE, et al. CNS myelin and sertoli cell tight junction strands are absent in Osp/claudin-11 null mice. Cell 1999;99:649–59.
[31] Tiwari-Woodruff SK, Buznikov AG, Vu TQ, Micevych PE, Chen K, Kornblum HI, et al. OSP/claudin-11 forms a complex with a novel member of the tetraspanin super family and beta1 integrin and regulates proliferation and migration of oligodendrocytes. Journal of Cell Biology 2001;153:295–305.
[32] Kruger RP, Lee J, Li W, Guan KL. Mapping netrin receptor binding reveals domains of Unc5 regulating its tyrosine phosphorylation. Journal of Neuroscience 2004;24:10826–34.
[33] Serafini T, Colamarino SA, Leonardo ED, Wang H, Beddington R, Skarnes WC, et al. Netrin-1 is required for commissural axon guidance in the developing vertebrate nervous system. Cell 1996;87:1001–14.
[34] Alcántara S, Ruiz M, De Castro F, Soriano E, Sotelo C. Netrin 1 acts as an attractive or as a repulsive cue for distinct migrating neurons during the development of the cerebellar system. Development 2000;127:1359–72.
[35] Spassky N, de Castro F, Le Bras B, Heydon K, Quéraud-LeSaux F, Bloch-Gallego E, et al. Directional guidance of oligodendroglial migration by class 3 semaphorins and netrin-1. Journal of Neuroscience 2002;22:5992–6004.
[36] Fazeli A, Dickinson SL, Hermiston ML, Tighe RV, Steen RG, Small CG, et al. Phenotype of mice lacking functional Deleted in colorectal cancer (Dcc) gene. Nature 1997;386:796–804.
[37] Rajasekharan S, Baker KA, Horn KE, Jarjour AA, Antel JP, Kennedy TE. Netrin 1 and Dcc regulate oligodendrocyte process branching and membrane extension via Fyn and RhoA. Development 2009;136:415–26.
[38] Forcet C, Ye X, Granger L, Corset V, Shin H, Bredesen DE, et al. The dependence receptor DCC (deleted in colorectal cancer) defines an alternative mechanism for caspase activation. Proceedings of the National Academy of Sciences of the United States of America 2001;98:3416–21.
[39] Furne C, Corset V, Hérincs Z, Cahuzac N, Hueber AO, Mehlen P. The dependence receptor DCC requires lipid raft localization for cell death signaling. Proceedings of the National Academy of Sciences of the United States of America 2006;103:4128–33.
[40] Mehlen P, Rabizadeh S, Snipas SJ, Assa-Munt N, Salvesen GS, Bredesen DE. The DCC gene product induces apoptosis by a mechanism requiring receptor proteolysis. Nature 1998;395:801–4.
[41] Sariola H, Saarma M. Novel functions and signalling pathways for GDNF. Journal of Cell Science 2003;116:3855–62.
[42] Strelau J, Unsicker K. GDNF family members and their receptors: expression and functions in two oligodendroglial cell lines representing distinct stages of oligodendroglial development. Glia 1999;26:291–301.
[43] Bordeaux MC, Forcet C, Granger L, Corset V, Bidaud C, Billaud M, et al. The RET proto-oncogene induces apoptosis: a novel mechanism for Hirschsprung disease. EMBO Journal 2000;19:4056–63.
[44] Pixley SK, de Vellis J. Transition between immature radial glia and mature astrocytes studied with a monoclonal antibody to vimentin. Brain Research 1984;317:201–9.
[45] Ciesielski-Treska J, Goetschy JF, Ulrich G, Aunis D. Acquisition of vimentin in astrocytes cultured from postnatal rat brain. Journal of Neurocytology 1988;17:79–86.
[46] Alonso G. Proliferation of progenitor cells in the adult rat brain correlates with the presence of vimentin-expressing astrocytes. Glia 2001;34:253–66.
[47] Pekny M, Wilhelmsson U, Bogestål YR, Pekna M. The role of astrocytes and complement system in neural plasticity. International Review of Neurobiology 2007;82:95–111.
[48] Eddleston M, Mucke L. Molecular profile of reactive astrocytes—implications for their role in neurologic disease. Neuroscience 1993;54:15–36.
[49] Sharlin DS, Bansal R, Zoeller RT. Polychlorinated biphenyls exert selective effects on cellular composition of white matter in a manner inconsistent with thyroid hormone insufficiency. Endocrinology 2006;147:846–58.

J Occup Health 2011; 53: 51–63

Journal of Occupational Health

Two- and 13-week Inhalation Toxicities of Indium-tin Oxide and Indium Oxide in Rats

Kasuke NAGANO[1], Kaoru GOTOH[1], Tatsuya KASAI[1], Shigetoshi AISO[1], Tomoshi NISHIZAWA[1], Makoto OHNISHI[1], Naoki IKAWA[1], Yoko EITAKI[2], Kenichi YAMADA[2], Heihachiro ARITO[1] and Shoji FUKUSHIMA[1]

[1]Japan Bioassay Research Center, Japan Industrial Safety and Health Association and [2]Occupational Health Research and Development Center, Japan Industrial Safety and Health Association, Japan

Abstract: Two- and 13-week Inhalation Toxicities of Indium-tin Oxide and Indium Oxide in Rats: Kasuke NAGANO, *et al.* Japan Bioassay Research Center, Japan Industrial Safety and Health Association—Objectives: Two- and 13-week inhalation toxicities of indium-tin oxide (ITO) and indium oxide (IO) were characterized for risk assessments of workers exposed to ITO. **Methods:** F344 rats of both sexes were exposed by inhalation to ITO or IO aerosol for 6 h/day, 5 day/wk for 2 wk at 0, 0.1, 1, 10 or 100 mg/m^3 or 13 wk at 0, 0.1or 1 mg/m^3. An aerosol generator and inhalation exposure system was constructed. **Results:** Blood and lung contents of indium were elevated in a dose-related manner in the ITO- and IO-exposed rats. ITO and IO particles were deposited in the lung, mediastinal lymph node and nasal-associated lymphoid tissue. Exposures to ITO and IO induced alveolar proteinosis, infiltrations of alveolar macrophages and inflammatory cells and alveolar epithelial hyperplasia in addition to increased lung weight. ITO affected the lung more severely than IO did. Fibrosis of alveolar wall developed and some of these lesions worsened at the end of the 26-week post-exposure period. **Conclusions:** Persistent pulmonary lesions including alveolar proteinosis and macrophage infiltration occurred after 2- and 13-week inhalation exposures of rats to ITO and IO. Fibrosis of alveolar wall developed later. These lesions occurred after ITO exposure at the same concentration as the current occupational exposure limit in the USA and at blood indium levels below the biological exposure index in Japan for indium.
(J Occup Health 2011; 53: 51–63)

Received Sep 17, 2010; Accepted Nov 15, 2010
Published online in J-STAGE Jan 11, 2011
Correspondence to: T. Nishizawa, Japan Bioassay Research Center, Japan Industrial Safety and Health Association, 2445 Hirasawa, Hadano, Kanagawa 257-0015, Japan
(e-mail: t-nishizawa@jisha.or.jp)

Key words: Indium-tin oxide, Indium oxide, Inhalation, Pulmonary toxicity, Rat

Indium-tin oxide (ITO), a sintered material containing 90% indium oxide (IO) and 10% tin oxide, has been extensively used in liquid-crystal displays and other display devices. The average annual growth of the use of indium in the form of ITO has increased by an average 18 percent per year[1]. The technology used to create ITO targets and ITO thin film applications gives rise to potential exposure to ITO particles, and poses a serious threat to the health of workers engaged in the manufacturing, processing and handling of ITO. Two fatal case studies have been reported. An operator of wet surface grinding in an ITO plant was diagnosed as interstitial pneumonia and died of bilateral pneumothorax[2], and a furnace operator in an ITO plant died of respiratory failure due to pulmonary alveolar proteinosis[3]. Recent epidemiological studies on the health of workers in ITO plants have demonstrated a potential cause of occupational lung disease as inhaled indium and an increased risk for interstitial lung damage by ITO inhalation[4–7]. Experimental toxicology studies have revealed that an administration of ITO causes persistent inflammation in the lung of rats[8], a strong cytotoxic response of macrophages *in vitro* by generation of reactive oxygen species (ROS)[8], and a pulmonary inflammatory response with diffuse bronchiolar and alveolar hyperplasia and interstitial fibrotic proliferation in hamsters[9,10]. An intratracheal administration of indium trichloride to rats was reported to initiate an inflammatory response with rapid development of fibrosis[11]. The National Toxicology Program's (NTP's) 14-week study[12] showed that inhalation exposure of rats to indium phosphide aerosol induces inflammation and alveolar proteinosis in the lung.

Inhalation is a principal route of exposure for workers in the facilities where ITO is manufactured, processed and

handled. In order to protect workers from inhalation exposure to indium and its compounds, an occupational exposure limit (OEL) of 0.1 mg/m^3 has been recommended as the Threshold Limit Value-Time Weighted Average (TLV-TWA) by the American Conference of Governmental Industrial Hygienists (ACGIH)[13], and as the Recommended Exposure Limit (REL) by the National Institute for Occupational Safety and Health (NIOSH)[14]. The Japan Society for Occupational Health (JSOH)[15] has recommended a serum indium level of 3 $\mu g/l$ as a biological exposure index (BEI). It is of prime importance to provide basic animal toxicity data showing the dose-response relationships between concentrations of inhalation exposure of rats and mice to ITO and its major component, IO, target tissue doses of indium and resulting pulmonary toxic responses to these two aerosols.

In order to assess the health risks of workers exposed by inhalation to ITO and IO aerosols in the work environment, the present studies were intended to characterize subacute and subchronic inhalation toxicities of ITO and IO in rats and to provide dose-response relationships between aerosol concentrations of inhalation exposure to ITO and IO aerosols, lung and blood contents of indium and resulting pulmonary lesions. For this purpose, we constructed an aerosol generation and exposure system for providing inhalation exposure of unrestrained rats and mice to aerosols of ITO and IO at strictly controlled exposure concentrations ranging from 0.1 to 100 mg/m^3. And, we conducted inhalation exposures of male and female rats to dry aerosols of ITO and IO at these concentrations for 2 and 13 wk. A further purpose of the present studies was to predict an appropriate range of exposure concentrations of ITO aerosol for a 2-year rodent carcinogenicity study, based on the results.

Materials and Methods

The present studies were conducted in accordance with the Organization for Economic Cooperation and Development's (OECD's) Good Laboratory Practice[16], and with reference to the OECD's Guidelines for Testing of Chemicals 412 "Repeated Dose Inhalation Toxicity, 28-day or 14-day Study"[17] and 413 "Subchronic Inhalation Toxicity, 90-day Study"[18]. The animals were cared for in accordance with the Guide for the Care and Use of Laboratory Animals[19] and the present studies were approved by the ethics committee of the Japan Bioassay Research Center.

Test materials

Powders of ITO and IO were kindly supplied by JX Nippon Mining & Metals, Corp. (former Nippon Mining & Metals Co., Ltd.) (Tokyo, Japan). ITO powder was prepared by grinding the sintered ITO plate, and was colored with black. The mean diameter of the powder was 3.5 μm with a 90% cumulative diameter of 8.9 μm. The sintered ITO powder was composed of 90.06% IO and 9.74% SnO_2. Its purity was 99.8% with trace amounts of aluminium, chromium, copper, iron, nickel, lead, silica, zirconium and zinc as impurities. IO powder was colored with yellow, and had a mean diameter of 1.4 μm with a 90% cumulative diameter of 2.9 μm. The purity of the IO powder was 99.9% with trace amounts of tin, silica and lead as impurities.

Animals

F344/DuCrlCrlj rats of both sexes were obtained at the age of 4 wk from Charles River Japan, Inc (Kanagawa, Japan). The animals were quarantined and acclimated for 2 wk before the start of experiment. The animals were housed individually in stainless-steel wire hanging cages (170 W × 294 D × 176 H mm), which were placed in a stainless steel inhalation exposure chamber of 1,060 liters in volume. The environment in the exposure chamber was maintained constant at a temperature of 20–24°C and a relative humidity of 30–70% with 12 air changes/h. The exposure chambers were installed in a barrier system animal room. Fluorescent lighting was controlled automatically to give a 12-hour light/dark cycle. All rats were given sterilized commercial pellet diet (CRF-1, Oriental Yeast Co., Ltd., Tokyo, Japan) and sterilized water *ad libitum*.

Experimental design

In the 2-week study, groups of 5 rats of each sex were exposed to ITO or IO aerosol at a target concentration of 0.1, 1, 10 or 100 mg/m^3 as ITO or IO for 6 h/day, 5 day/wk for 2 wk. In the 13-week study, groups of 10 rats of each sex were exposed to ITO or IO aerosol at a target concentration of 0.1 or 1 mg/m^3 for 6 h/day, 5 day/wk for 13 wk. Groups of 5 or 10 rats of each sex were exposed to clean air for 2 or 13 wk under the same conditions, and served as respective controls. In order to evaluate recovery from the subchronic effects after cessation of the 13-week exposure to ITO, a post-exposure group of 10 rats of each sex was set up, which was exposed to ITO at 0.1 mg/m^3 for 13 wk and then to clean air for 26 wk. Ten rats of each sex serving as respective controls were handled in the same manner as the post-exposure group, but were exposed to clean air for 39 wk.

Aerosol generation and exposure to ITO and IO

Two different systems for generation of ITO or IO aerosol and inhalation exposure were used in the present studies. A target aerosol concentration of 100 mg/m^3 was generated using a system illustrated in the upper part (A) of Fig. 1. It consisted of a dust feeder equipped with an ejector, an exposure chamber and a digital dust indicator (Type AP-632T, Sibata Scientific Technology, Ltd., Tokyo, Japan). Airflow containing the aerosol was generated by drawing the powder with compressed clean air at the first

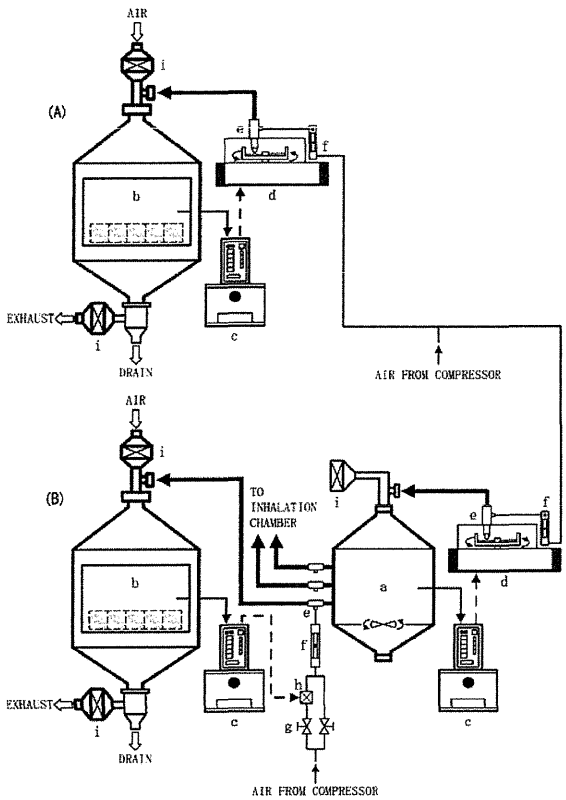

Fig. 1. A schematic diagram of the aerosol generation, regulation and inhalation exposure systems. (A) A system used for aerosol generation of a high aerosol concentration of 100 mg/m^3. (B) Another system used for generation of lower concentrations of 10, 1 and 0.1 mg/m^3. Thick, thin and dotted arrows indicate aerosol flow, sampling of chamber air for monitoring aerosol concentration and feedback control, respectively. Components of the systems: a) reservoir chamber, b) inhalation exposure chamber, c) digital dust indicator, d) dust feeder with an ejector, e) ejector, f) flowmeter, g) flow control valve, h) solenoid valve, i) HEPA filter.

ejector and introduced into the top of the exposure chamber where the filtered air had been kept flowing downward at 12 air changes/h. The mass-equivalent concentration of ITO or IO in the exposure chamber was monitored with the digital dust indicator. In order to keep the aerosol concentration constant in the exposure chamber during the 6-hour exposure period, a feedback control system between the digital dust indicator and the dust feeder was set up. When the chamber concentration went above an upper limit of a normal concentration range, the dust feeder stopped supplying the powder. Conversely, when the chamber concentration fell below the lower limit, the dust feeder started to supply the powder. Chamber concentrations of 10, 1 and 0.1 mg/m^3 were generated using another system illustrated in the lower part (B) of Fig. 1. It consisted of the first-stage system (a, c and d in Fig. 1B) for aerosol generation of a high concentration at 100 mg/m^3 and a further dilution system. Aerosol generation of the high concentration and its regulation were performed in the same manner described above, and airflow containing the aerosol was delivered to a reservoir chamber for stabilization of the aerosol concentration. The airflow containing the aerosol was delivered to the second ejector and then introduced into the top of the exposure chambers where the filtered air had been kept flowing downward at 12 air changes/h. The aerosol concentration in the exposure chamber was monitored with the second digital dust indicator and regulated at a target concentration of 10, 1 or 0.1 mg/m^3. The aerosol concentration was stabilized by setting up the second feedback system between the digital dust indicator and a solenoid valve which regulated the flow rate of compressed clean air entering the second ejectors. The exposure chambers were kept at a negative pressure (–100 Pa), in order to prevent leakage of ITO and IO aerosols into the outside air. Exhaust air from the exposure chamber was passed through a HEPA filter to remove ITO and IO particles before release into the atmosphere. The concentrations of indium in the exhaust air were below the detection limit of 0.0001 mg/m^3 after the treatment with the HEPA filter.

Chamber concentrations and size distribution of ITO and IO aerosols

In order to determine concentrations of ITO or IO aerosol in the exposure chamber, ITO or IO particles were collected on a filter (Teflon binder T60A20, Sibata Scientific Technology, Ltd, Tokyo, Japan) on Days 1 and 8 in the 2-week study and every week in the 13-week study. The particles on the filter were dissolved in a mixture solution of distilled water, hydrochloric acid and nitric acid (2:2:1 by volume ratio) at 160°C. The resulting solution was diluted with nitric acid, and then subjected to atomic absorption spectrometry analysis (Polarized Zeeman Atomic Absorption Spectrophotometer, Z-5010, Hitachi High-Technol. Co., Tokyo, Japan). Exposure chamber concentrations of ITO and IO aerosols were derived from the measured levels of elemental indium as shown in Table 1.

Measurement of the size distribution of ITO or IO aerosol in the exposure chamber was carried out once in the 2-week study and in the 4th and 8th wk in the 13-week study. ITO or IO aerosol was collected with an 8-stage Andersen sampler (Type AN200, Sibata Scientific Technology, Ltd). Using the mass of the particles on the filter (Teflon binder T60A20, Sibata Scientific Technology, Ltd) collected at each stage of the Andersen sampler, mass median aerodynamic diameter (MMAD) and geometric standard deviation (GSD) were determined.

Table 1. Mass concentrations and mass median aerodynamic diameters (MMADs) and geometric standard deviations (GSDs) of ITO and IO aerosols in the exposure chamber

	ITO				IO			
	Mass concentration (mg/m^3)		Aerodynamic diameter		Mass concentration (mg/m^3)		Aerodynamic diameter	
Dose	(Mean ± SD)		Median (μm)	GSD	(Mean ± SD)		Median (μm)	GSD
2-week study		In a)				In a)		
0.1 mg/m^3	0.09 ± 0.00	0.07 ± 0.00	2.5	1.8	0.10 ± 0.01	0.08 ± 0.01	1.9	1.7
1 mg/m^3	0.94 ± 0.02	0.70 ± 0.01	2.7	1.8	1.07 ± 0.06	0.89 ± 0.05	2.1	1.8
10 mg/m^3	9.33 ± 0.33	6.94 ± 0.25	3.0	1.8	10.76 ± 0.46	8.90 ± 0.38	2.1	1.8
100 mg/m^3	95.90 ± 2.99	71.35 ± 2.22	3.7	1.9	105.25 ± 7.01	87.04 ± 5.80	2.2	1.7
13-week study								
0.1 mg/m^3	0.10 ± 0.01	0.07 ± 0.01	2.4	1.8	0.10 ± 0.01	0.08 ± 0.01	2.1	1.7
1 mg/m^3	1.01 ± 0.08	0.75 ± 0.06	2.5	1.9	1.01 ± 0.09	0.84 ± 0.07	2.3	1.7

a): Mass concentration as indium.

Determination of indium concentrations in the lung and blood

Lung indium was quantified in the 2-week study, and both the lung and whole-blood were analyzed for indium in the 13-week study. Cranial, caudal and accessory lobes of the right lung were used for the analysis. A sample of the lung or 1.0 m*l* of blood was added with ultra-pure nitric acid and digested with a microwave digestion apparatus (Microwave Digestion System, Model 7295, O·I·Analytical, CA, USA). The digested sample was added with ultra-pure water and injected into an inductively coupled plasma mass spectrometer (ICP-MS) (Type 7500i, Agilent Technologies, Ltd., CA, USA). Cesium was used as an internal standard for the indium measurement. The quantitative detection limit of indium was 0.006 $\mu g/g$ for lung tissue and 0.5 $\mu g/l$ for whole-blood. Lung indium was expressed as both a concentration of indium per gram of lung tissue and the content of indium in the whole-lung.

Clinical observations and pathological examinations

The animals were observed daily for their clinical signs and mortality. Body weight and food consumption were measured weekly throughout the study periods. Animals surviving to the end of the 2- or 13-week exposure period and to the end of the 26-week post-exposure period received complete necropsy. Blood was collected for blood indium, hematology and blood biochemistry from the abdominal aorta under etherization. The organs and tissues designated in the OECD test guidelines[17, 18] were examined macroscopically and microscopically. The tissues were fixed in 10% neutral buffered formalin, and embedded in paraffin. Tissue sections of 5 μm in thickness were prepared, and stained with hematoxylin and eosin (H & E). The sections of lung tissue were also stained with a periodic acid Schiff (PAS) reagent. Lesions of the lung and lymph nodes were evaluated for their severities, scoring on a scale of "slight" to "severe" with reference to the criteria of non-neoplastic lesions by Shackelford *et al.*[20].

Statistical analysis

Body weight, organ weight, and hematological and blood biochemical parameters were analyzed by Dunnett's test as described previously[21]. Histopathological findings in the 13-week study were analyzed by chi-square test. A two-tailed test was used for all statistics. In all cases, a p value of 0.05 was used as the level of significance.

Results

Exposure chamber concentrations and size distributions of ITO and IO aerosol

Table 1 shows the mass concentrations derived from the measured levels of elemental indium (mean ± SD), MMADs and GSDs of ITO and IO aerosols in the exposure chamber. The exposure concentrations of ITO and IO aerosols were found to be regulated precisely within less than 10% in the variation coefficient and accurately within less than 10% deviation from the target concentrations. MMADs of the ITO aerosol tended to slightly increase with an increase in the chamber concentrations, while the GSDs were constant at all exposure concentrations. On the other hand, MMADs and GSDs of IO aerosol were constant over a wide range of exposure concentrations, and MMADs of IO aerosol were slightly smaller than those of ITO aerosol.

Indium concentrations in the lung and blood

Table 2 shows lung and blood contents of indium in the male and female rats exposed to ITO and IO for 2 and 13 wk. Lung contents of indium expressed as $\mu g/g$ lung tissue and μg/whole-lung were increased with an increase in the concentration of exposure to ITO or IO, but the exposure concentration-related increase was smaller in the unit of $\mu g/g$ lung tissue than in that of μg/whole-lung, because the lung weights of the exposed rats were significantly heavier, up to 2-fold heavier than those of the control groups, depending on the exposure concentration (Fig. 2). In the 2-week study, the whole-lung contents of indium in the

Table 2. Lung and blood contents of indium in the male and female rats exposed to ITO or IO at 4 different concentrations for 2 wk, in those exposed to ITO or IO at 0.1 or 1 mg/m^3 for 13 wk, and in those exposed to ITO at 0.1 mg/m^3 for 13 wk followed by exposure to clean air for 26 wk

	2-week study				13-week study		
Group name (mg/m^3)	0.1	1	10	100	0.1	0.1 (P)	1
No. of animals examined	5	5	5	5	10	10	10
<ITO>							
Male							
Lung (μg/g as In)	3.3 ± 0.3	32.4 ± 2.7	127.6 ± 17.7	470.3 ± 58.1	24.0 ± 2.7	8.8 ± 1.1	74.4 ± 10.5
Lung (μg/whole-lung as In)	2.4 ± 0.1	31.1 ± 1.8	165.1 ± 9.8	688.3 ± 43.1	38.7 ± 4.6	15.0 ± 2.0	173.9 ± 28.6
Blood (μg/*l* as In)	–	–	–	–	0.77 ± 0.09	1.04 ± 0.10	3.39 ± 0.33
Female							
Lung (μg/g as In)	2.9 ± 0.4	34.8 ± 8.8	148.0 ± 41.2	533.9 ± 69.1	22.9 ± 2.2	8.6 ± 1.0	79.9 ± 7.1
Lung (μg/whole-lung as In)	1.8 ± 0.2	28.1 ± 7.2	157.4 ± 41.9	658.7 ± 70.9	26.3 ± 2.7	10.3 ± 1.1	134.6 ± 8.0
Blood (μg/*l* as In)	–	–	–	–	1.13 ± 0.32	1.46 ± 0.26	4.06 ± 0.56
<IO>							
Male							
Lung (μg/g as In)	5.3 ± 0.5	61.3 ± 11.1	261.7 ± 7.2	1124.7 ± 49.3	18.0 ± 2.3	–	144.2 ± 15.7
Lung (μg/whole-lung as In)	3.7 ± 0.3	45.1 ± 5.7	324.5 ± 20.0	1689.2 ± 64.2	17.2 ± 2.8	–	235.5 ± 34.0
Blood (μg/*l* as In)	–	–	–	–	ND	–	0.76 ± 0.08
Female							
Lung (μg/g as In)	5.0 ± 0.3	52.8 ± 3.2	267.0 ± 25.5	1190.8 ± 51.0	13.4 ± 1.5	–	130.6 ± 15.7
Lung (μg/whole-lung as In)	3.1 ± 0.2	33.8 ± 3.2	263.8 ± 26.7	1464.1 ± 88.2	9.8 ± 1.0	–	157.3 ± 17.4
Blood (μg/*l* as In)	–	–	–	–	ND	–	0.96 ± 0.26

(P): Data at the end of the 26-week post-exposure period. Values indicate mean ± SD. ND: Contents were below the quantitative detection limit (0.5 μg/*l*). –: Not examined.

ITO- and IO-exposed groups of both sexes were not increased in a manner proportional to the exposure concentration. The whole-lung contents of indium were lower in the ITO-exposed groups than in the IO-exposed groups of both sexes at all exposure concentrations. In the 13-week study, the exposure concentration-related increase in the whole-lung content of indium was also disproportionately lowered to greater extent in the ITO-exposed rats than in the IO-exposed rats. Unlike the result from the 2-week study, the whole-lung contents of indium in the 0.1 mg/m^3 ITO-exposed rats of both sexes were higher than those of the 0.1 mg/m^3 IO-exposed rats of both sexes. The whole-lung contents of indium in the ITO-exposed rats of both sexes measured at the end of the 26-week post-exposure period were lowered to 40% as compared with those measured at the end of the 13-week exposure.

Table 2 also shows the blood contents of indium in the male and female rats at the end of 13-week exposures to ITO and IO at 0.1 and 1 mg/m^3 as well as those exposed to ITO at 0.1 mg/m^3 for 13 wk and then to clean air for 26 wk. The blood contents of indium in the 0.1 mg/m^3 IO-exposed rats of both sexes were below the quantitative detection limit of 0.5 μg/*l*. The blood contents of indium in the 1 mg/m^3 ITO-exposed groups of both sexes were 4-fold higher than those in 1 mg/m^3 IO-exposed group of both sexes. The blood contents of indium in the 0.1 mg/m^3 ITO-exposed rats of both sexes measured at the end of the 26-week post-exposure period were 1.3-fold higher than those measured at the end of the 13-week exposure period.

Mortality and clinical signs in the 2- and 13-week studies

Neither death nor abnormal clinical sign, such as irregular sounds of respiration, was observed in any group exposed to ITO or IO for 2 or 13 wk. There was no growth retardation in any group exposed to ITO or IO for 2 or 13 wk as compared with the growth rate in the respective control.

Hematological and blood biochemical changes in the 2- and 13-week studies

In the 2-week study, white blood cell counts in the 100

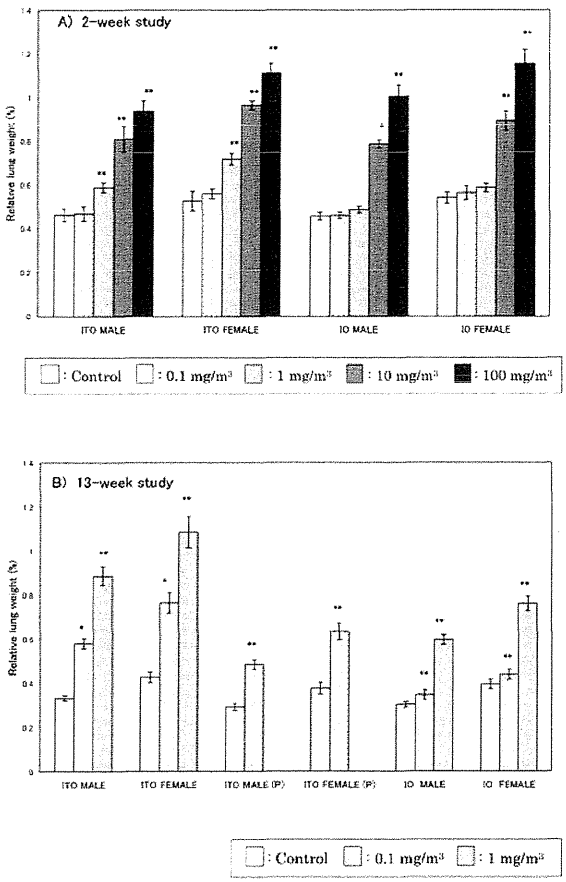

Fig. 2. Relative lung weights: A) in the rats of both sexes exposed to ITO or IO aerosol at 0, 0.1, 1, 10 or 100 mg/m^3 for 2 wk, B) in the rats of both sexes exposed to ITO or IO aerosol at 0, 0.1 or 1 mg/m^3 for 13 wk. (P) represents the rats of both sexes exposed to ITO aerosol at 0 or 0.1 mg/m^3 for 13 wk and subsequently to clean air for 26 wk.

mg/m^3 ITO-exposed male rats and red blood cell counts, hemoglobin and hematocrit values in the 100 mg/m^3 IO-exposed male rats were significantly increased compared with the respective control groups. In the 13-week study, potassium was significantly decreased in both 0.1 and 1 mg/m^3 ITO- and IO-exposed rats. In addition, significant decreases in sodium and chlorine in the 0.1 and 1 mg/m^3 IO-exposed male rats and significantly decreased triglyceride in the 0.1 and 1 mg/m^3 IO-exposed female rats were also observed (data not shown).

Pathological findings in the 2-week study

Relative lung weights were significantly increased in the male and female rats exposed to ITO at 1 mg/m^3 and above compared with the respective control groups, whereas significantly increased lung weights were noted in the rats of both sexes exposed to IO only at 10 and 100 mg/m^3 compared with the respective control groups (Fig. 2-A). Increases in absolute lung weights were indicated as well (data not shown).

Microscopic examination revealed that ITO and IO particles were deposited in the lungs of all the exposed rats except those exposed to the 0.1 mg/m^3 (Table 3). The particles were pale brown and transparent, looked like amber, and were located primarily within the alveolar macrophages (Fig. 3-1) and partly as a free form in the alveolar space. Both ITO and IO particles were deposited separately as single particles. ITO and IO particles were also observed to lesser extent in the bronchus-associated lymphoid tissue (BALT) of the lung, in the mediastinal lymph nodes (MLN) and in the nasal-associated lymphoid tissue (NALT) of the nasopharyngeal duct. The particles were located within macrophages, and notably, degenerative alveolar macrophages engulfing the particles were often observed (Fig. 3-1). The most remarkable lesion found in the present 2-week study was alveolar proteinosis characterized by filling of the alveolar space with a granular, pale eosinophilic material in the ITO- and IO-exposed rats. The diagnosis of alveolar proteinosis was based on the positive staining of eosinophilic material in the alveolar space with a PAS reagent. Alveolar proteinosis was observed in the 1, 10 and 100 mg/m^3 ITO-exposed rats and in the 10 and 100 mg/m^3 IO-exposed rats, and its severity score was increased dose-dependently in both the ITO- and IO-exposed groups. Incidences of alveolar macrophage infiltration in the ITO and IO-exposed rats were increased at the same exposure concentrations as the occurrence of alveolar proteinosis. Infiltration of inflammatory cells which were primarily composed of neutrophils and lymphocytes was observed in the alveolar space and wall of almost all the 10 and 100 mg/m^3 ITO- and IO-exposed rats of both sexes. Hyperplasia of alveolar epithelium occurred in some 10 and 100 mg/m^3 ITO- and IO-exposed rats, and was characterized by increased numbers of cuboidal cells, which were assumed to be type II pneumocytes, and by their location in the focal lung areas accompanied by infiltrations of alveolar macrophages and inflammatory cells. Those alveolar macrophages had foamy cytoplasm.

Pathological findings in the 13-week study

Relative lung weights were significantly increased in all the rats of both sexes exposed to ITO and IO at 0.1 and 1 mg/m^3 compared with the respective control groups (Fig. 2-B). The increase in the relative lung weight was more marked in the ITO-exposed rats of both sexes than in the IO-exposed rats. Increases in absolute lung weights were observed as well (data not shown).

Microscopic examination revealed that ITO and IO particles were deposited in the lungs of all the exposed

Table 3. Histopathological findings in the lung and lymph nodes of male and female rats exposed to ITO or IO at 4 different concentrations or clean air for 2 wk

	ITO					IO				
Group name (mg/m³)	Control	0.1	1	10	100	Control	0.1	1	10	100
No. of animals examined	5	5	5	5	5	5	5	5	5	5
<Male>										
Deposition of particles										
Lung	0	0	5	5	5	0	0	5	5	5
BALT	0	0	0	1	5	0	0	0	3	5
MLN	0	0	0	2	5	0	0	0	3	5
NALT	0	0	0	1	5	0	0	0	5	5
Histopathological findings										
Lung										
Alveolar proteinosis	0	0	5	5	5	0	0	0	5	5
			<1.0>	<2.0>	<2.0>				<1.8>	<2.0>
Infiltration of alveolar macrophages	0	0	5	5	5	0	0	0	5	5
			<1.0>	<1.0>	<1.0>				<1.0>	<1.0>
Infiltration of inflammatory cells	0	0	0	5	5	0	0	0	4	5
				<1.2>	<1.0>				<1.3>	<1.2>
Hyperplasia of alveolar epithelium	0	0	0	3	4	0	0	0	3	1
				<1.0>	<1.0>				<1.0>	<1.0>
<Female>										
Deposition of particles										
Lung	0	0	5	5	5	0	0	5	5	5
BALT	0	0	0	0	4	0	0	0	3	5
MLN	0	0	0	2	3	0	0	0	3	5
NALT	0	0	0	0	3	0	0	0	3	3
Histopathological findings										
Lung										
Alveolar proteinosis	0	0	5	5	5	0	0	0	5	5
			<1.0>	<2.0>	<2.0>				<1.8>	<2.0>
Infiltration of alveolar macrophages	0	0	5	5	5	0	0	2	5	5
			<1.0>	<1.0>	<1.0>			<1.0>	<1.0>	<1.0>
Infiltration of inflammatory cells	0	0	1	5	5	0	0	0	5	5
			<1.0>	<1.2>	<1.0>				<1.0>	<1.0>
Hyperplasia of alveolar epithelium	0	0	0	3	2	0	0	0	3	0
				<1.0>	<1.0>				<1.0>	

Values indicate number of animals bearing lesions. The values in angle bracket indicate the average of severity grade index of the lesion. The average of severity grade is calculated with a following equation. Σ(grade × number of animals with grade) / number of affected animals. Grade: 1, slight; 2, moderate; 3, marked; 4, severe. BALT: Bronchus-associated lymphoid tissue. MLN: Mediastinal lymph nodes. NALT: Nasal-associated lymphoid tissue.

rats of both sexes (Table 4). The particles were located primarily within the alveolar macrophages and partly as a free form within the alveolar space. ITO and IO particles were also observed to a lesser extent in the BALT of the 0.1 and 1 mg/m³ ITO- exposed and 1 mg/m³ IO-exposed rats, in the MLN of both 0.1 and 1 mg/m³ ITO- and IO-exposed rats, and in the NALT of the 1 mg/m³ ITO- and IO-exposed rats. Alveolar proteinosis occurred in all the ITO-exposed rats and in the 1 mg/m³ IO-exposed rats (Fig. 3-2). The severity score of alveolar proteinosis of the 0.1 mg/m³ ITO-exposed rats was equal to that of the 1 mg/m³ IO-exposed rats. Infiltration of alveolar macrophages was observed in the 0.1 and 1 mg/m³ ITO- and IO-exposed rats. Notably, swelling of cytoplasm in the alveolar macrophages was evidently recognized, indicating degeneration of the macrophages. Some alveolar macrophages contained PAS-positive, eosinophilic material in the cytoplasm. A significant increase in

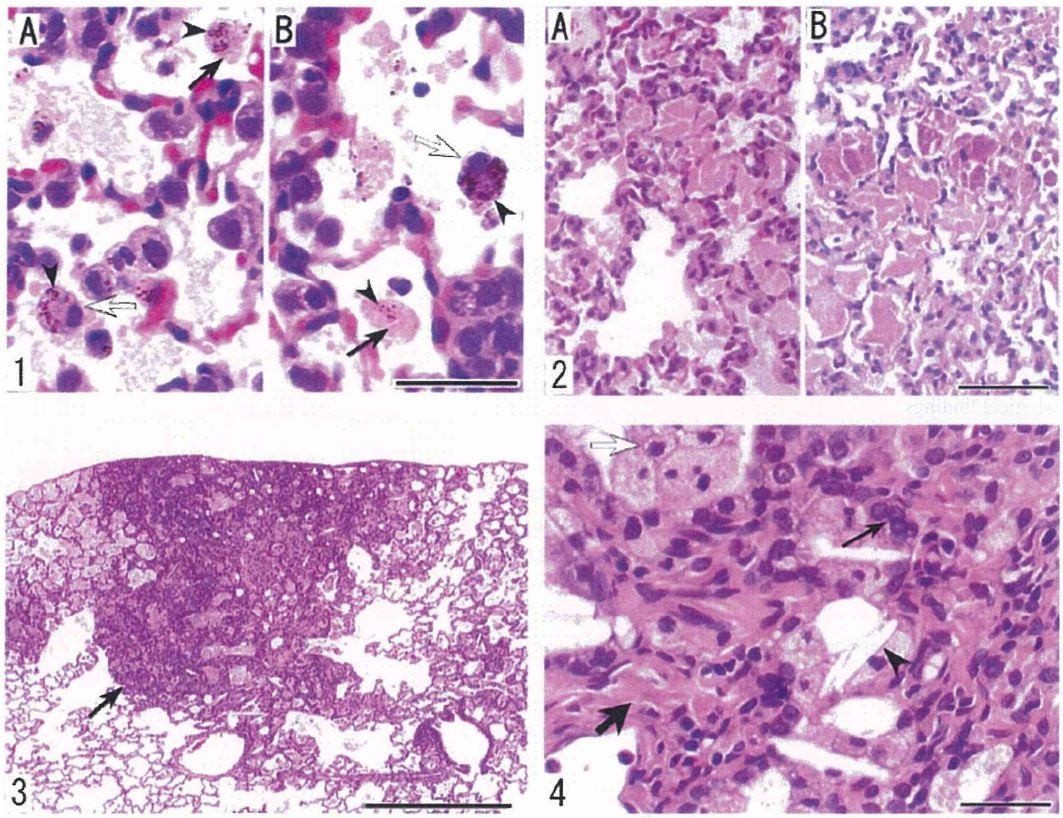

Fig. 3. 1) Microphotographs showing the presence of particles (arrowheads) in the alveolar macrophages in the lung of a male rat exposed to ITO at 100 mg/m^3 for 2 wk (A) and in the lung of another rat exposed to IO at 100 mg/m^3 for 2 wk (B). Note that alveolar macrophages engulfing the particles (open arrows) are degenerative (filled arrows). H & E stain. Bar indicates 50 μm. 2) Microphotographs showing alveolar proteinosis in the lung of a male rat exposed to ITO at 0.1 mg/m^3 for 13 wk, stained with H & E (A) and in the lung of the same rat stained with a PAS reagent (B). Bar indicates 100 μm. 3) A microphotograph showing a low power view of a focal lesion (arrow) located beneath the pleural wall in a male rat exposed to ITO at 0.1 mg/m^3 for 13 wk and then exposed to clean air for 26 wk. H & E stain. Bar indicates 500 μm. 4) A microphotograph showing a high power view of alveolar wall fibrosis, alveolar epithelial hyperplasia, and alveolar macrophage infiltration in a male rat exposed to ITO at 0.1 mg/m^3 for 13 wk and then exposed to clean air for 26 wk. Note the alveolar wall fibrosis indicating an increase in collagen-like connective tissue (thick filled arrow), hyperplasia of alveolar epithelium (thin filled arrow), cholesterol cleft (arrowhead) and swelling of cytoplasm in alveolar macrophages (open arrow). H & E stain. Bar indicates 50 μm.

inflammatory cell infiltration was observed in the 1 mg/m^3 ITO- and IO-exposed rats, and these incidences were higher in the ITO-exposed rats than in the IO-exposed rats. Hyperplasia of alveolar epithelium occurred mainly in some rats exposed to ITO at 0.1 mg/m^3 and in the 1 mg/m^3 IO-exposed rats. Small granulomas composed of particle-laden macrophages were observed in the MLN of the 0.1 and 1 mg/m^3 ITO-exposed rats and in the 1 mg/m^3 IO-exposed rats.

Pathological findings at the end of the 26-week post-exposure period

Relative lung weights were significantly increased in the exposed rats at the end of the 26-week post-exposure period as compared with those of respective controls (denoted as (P) in Fig. 2-B).

Microscopic examination revealed the presence of ITO particles in the lung, BALT and MLN of the exposed rats at the end of the 26-week post-exposure period (denoted as (P) in Table 4). All the lesions seen in the lung and lymph nodes/tissue of the 0.1 mg/m^3 ITO-exposed group at the end of the 13-week exposure period persisted throughout the 26-week post-exposure period. A focal lesion composed of alveolar wall fibrosis, alveolar epithelial hyperplasia, infiltrations of alveolar macrophages and inflammatory cells was observed beneath the pleural

Table 4. Histopathological findings in the lung and lymph nodes of male and female rats exposed to ITO or IO at 0, 0.1 or 1 mg/m^3 for 13 wk, or exposed to ITO at 0.1 mg/m^3 for 13 wk followed by exposure to clean air for 26 wk

	ITO					IO		
	13 wk			13 wk (*P*)		13 wk		
Group name (mg/m^3)	Control	0.1	1	Control	0.1	Control	0.1	1
No. of animals examined	10	10	10	10	10	10	10	10
<Male>								
Deposition of particles								
Lung	0	10	10	0	10	0	10	10
BALT	0	9	9	0	7	0	0	10
MLN	0	7	9	0	9	0	0	10
NALT	0	0	2	0	0	0	0	2
Histopathological findings								
Lung								
Alveolar proteinosis	0	10 ** <2.0>	10 ** <3.0>	0	10 ** <1.7>	0	0	10** <2.0>
Infiltration of alveolar macrophages	0	10 ** <1.1>	10 ** <2.0>	0	10 ** <1.3>	0	6 * <1.0>	10** <1.0>
Infiltration of inflammatory cells	0	2 <1.0>	10 ** <1.0>	0	4 <1.0>	0	0	5 * <1.0>
Hyperplasia of alveolar epithelium	0	2 <1.0>	0	0	10 ** <1.3>	0	0	6 * <1.0>
Granuloma of BALT	0	0	1 <1.0>	0	0	0	0	0
Fibrosis of alveolar wall	0	0	0	0	10 ** <1.0>	0	0	0
Thickening of pleura	0	0	0	0	0	0	0	0
Lymph nodes								
Granuloma of MLN	0	5 * <1.0>	7 ** <1.0>	0	5 * <1.0>	0	0	5 * <1.0>

(P): Data at the end of the 26-week post-exposure period. Note: Values indicate number of animals bearing lesions. The values in angle bracket indicate the average of severity grade index of the lesion. The average of severity grade is calculated with a following equation. Σ(grade × number of animals with grade) / number of affected animals. Grade: 1, slight; 2, moderate; 3, marked; 4, severe. Significant difference: *, $p \leq 0.05$; **, $p \leq 0.01$ by Chi-square test. BALT: Bronchus-associated lymphoid tissue. MLN: Mediastinal lymph nodes. NALT: Nasal-associated lymphoid tissue.

wall (Fig. 3-3 and -4). Fibrosis of alveolar wall in all the exposed rats and thickening of pleural wall in one exposed female rat were evidently recognized only at the end of the 26-week post-exposure period, and were characterized by an increase in collagen-like connective tissue in the alveolar (Fig. 3-4) and pleural wall, respectively. It was noteworthy that cholesterol cleft (Fig. 3-4) was often observed in the same alveolar region at the end of the 26-week post-exposure period. The incidences and severities of alveolar epithelial hyperplasia were increased in the 26-week post-exposure groups as compared with that at the end of the 13-week exposure period.

No exposure-related histopathological changes were observed in any other organ or tissue in the ITO- or IO-exposed rats of either sex in the 2- and 13-week studies or at the end of the 26-week post-exposure period.

Discussion

The present system of aerosol generation and inhalation exposure was found to generate ITO and IO aerosols at the reproducible exposure concentrations regulated precisely within 10% coefficient of variation and accurately within 10% deviation from the target concentrations. Thus, this system allows to repeatedly expose individually housed, unrestrained rats of both sexes to ITO or IO particles of micron size at a wide range of concentrations from 0.1 to 100 mg/m^3 in large inhalation exposure chambers (1 m^3) for a time period of up to 90 days. The aerosols of ITO and IO in the exposure chamber were not aggregated and were well-dispersed to single particles of about 2–3 μm in

Table 4. continued

	ITO					IO		
	13 wk			13 wk (P)		13 wk		
Group name (mg/m³)	Control	0.1	1	Control	0.1	Control	0.1	1
No. of animals examined	10	10	10	10	10	10	10	10
<Female>								
Deposition of particles								
Lung	0	10	10	0	10	0	10	10
BALT	0	3	10	0	10	0	0	10
MLN	0	9	10	0	7	0	2	10
NALT	0	0	6	0	0	0	0	3
Histpothological findings								
Lung								
Alveolar proteinosis	0	10 ** <2.0>	10 ** <3.0>	0	10 ** <1.9>	0	0	10** <2.0>
Infiltration of alveolar macrophages	0	10 ** <1.0>	10 ** <2.0>	0	10 ** <1.5>	0	2 <1.0>	10** <1.0>
Infiltration of inflammatory cells	0	2 <1.0>	10 ** <1.0>	0	10 ** <1.0>	0	0	7 ** <1.0>
Hyperplasia of alveolar epithelium	0	5 * <1.0>	1 <1.0>	0	10 ** <1.4>	0	0	7 ** <1.0>
Granuloma of BALT	0	0	0	0	4 <1.0>	0	0	0
Fibrosis of alveolar wall	0	0	0	0	10 ** <1.0>	0	0	0
Thickening of pleura	0	0	0	0	1 <1.0>	0	0	0
Lymph nodes								
Granuloma of MLN	0	4 <1.0>	8 ** <1.0>	0	4 <1.0>	0	0	2 <1.0>

MMAD. The inhalation exposures of rats to the well-dispersed aerosols of ITO and IO resulted in depositions of ITO and IO particles in the alveolar region, which were detected in all exposed rats, except for those exposed to 0.1 mg/m³ for 2 wk. In addition, ITO and IO particles were deposited in the BALT, MLN and NALT of the exposed rats, but the extent of deposition was less in the lymph tissues and nodes than in the alveolar region. Light-microscopic examination of particle deposition in the lung and lymph nodes revealed that the particles were deposited separately as single particles.

It is interesting to note that the blood contents of indium in the male and female rats exposed to ITO at 1 mg/m³ for 13 wk were increased by 4.5- and 4.2-fold relative to the corresponding IO-exposed males and females, respectively, and that the blood contents of indium in the male and female rats exposed to 0.1 mg/m³ ITO were 0.77 and 1.13 $\mu g/l$, respectively, whereas the blood indium levels in the 0.1 mg/m³ IO-exposed rats of both sexes were below the detection limit of 0.5 $\mu g/l$. This finding can be interpreted as indicating that ITO particles are dissolved to greater extent in the deep lung than IO, resulting in higher blood contents of indium in the ITO-exposed rats. Kabe *et al.*[22] demonstrated that indium phosphide powder is clearly soluble in synthetic gastric fluid indicative of acidic pH, while the powder is insoluble in saline or synthetic lung fluid (Gamble solution). Dittmar *et al.*[23] reported that when indium phosphide particles are exposed to Gamble solution, a complex dynamic interaction with the particle surface results in high levels of dissolved indium. Brain *et al.*[24] suggested that insoluble metal particles contained in phagolysosomes of an alveolar macrophage are dissolved, because of the acidic environment (pH–4.8) in the phagolysosomes. The enhanced solubility of ITO particles in alveolar macrophages of the ITO-exposed rats warrants a further study.

The elemental or ionic form of indium leached from ITO particles is considered to play an important role in the induction of indium toxicity. Suzuki and Matsushita[25] showed that interaction of various metallic ions with surface pressure of phospholipid monolayer mimicking a biomembrane is positively correlated with acute lethal

doses of metal chlorides in rats and rabbits, and that indium ions interact most strongly with the simulated biomembrane causing possible impairment of cellular integrity. Blazka *et al.*[11] demonstrated that a single intratracheal administration of indium chloride dissolved in saline (pH 4.1) induces persistent inflammatory responses and development of fibrosis in rats. Lison *et al.*[8] reported that a strong cytotoxic response to ITO particles is induced *in vitro* in macrophages (NR8383 cell line) but not in rat lung epithelial cells. Taken together, it is likely that indium leached from ITO particles in the alveolar macrophages might be involved in the cellular disintegrity of alveolar macrophages, since degenerative alveolar macrophages with swollen cytoplasm engulfing ITO and IO particles were observed microscopically in the present 2- and 13-week studies.

Subacute pulmonary toxicity induced by the 2-week exposure to ITO was characterized by alveolar proteinosis, macrophage infiltration, inflammatory cell infiltration and alveolar epithelial hyperplasia. The former two pulmonary lesions occurred at exposures of 1 mg/m^3 and above, while the latter two appeared primarily at exposures of 10 and 100 mg/m^3. The 13-week inhalation exposure to ITO was found to induce essentially the same pulmonary lesions as those observed in the 2-week exposure, but at lower exposure concentrations. Furthermore, the histopathological examination at the end of the 26-week post-exposure period revealed development of fibrosis of alveolar wall, worsening of alveolar epithelial hyperplasia and persistence of the pulmonary lesions observed at the end of the 13-week exposure to ITO. No recovery from the subchronic effects of indium was indicated. Therefore, the present findings indicate that the pulmonary toxicity of inhaled ITO particles is more severe than that of IO particles and that alveolar macrophages play a critically important role in the induction of indium toxicity as evidenced by alveolar proteinosis, alveolar macrophage infiltration and swollen alveolar macrophages engulfing the particles, all of which occur at the lowest exposure concentration. Lison *et al.*[8] compared *in vivo* and *in vitro* pulmonary toxicity of ITO particles with those of its constituents, tin-oxide, IO and their unsintered mixture. They attributed the reactivity/toxicity of sintered ITO particles to carbon centered radical formation and Fenton-like activity, appearing with a high electron density of the sintering process through which TO molecules were introduced within crystal structure of IO[26]. However, it can be inferred from the present 2-week and 13-week studies that these pulmonary lesions are not causally linked to the dust overload induced by excessive inhalation exposure to ITO or IO aerosol, since the whole-lung contents of indium in the ITO- or IO-exposed rats were far below the levels of dust burden causing overloading, which are reported to be greater than 1–2 mg of persistently retained dust in the lungs of F344 rats[27].

The most remarkable pulmonary lesion found in the present studies was alveolar proteinosis accompanied by alveolar macrophage infiltration. These two lesions were the most sensitive, appearing at the lowest exposure concentration. The alveolar proteinosis observed in the lung of rats exposed to ITO and IO aerosols were characterized by filling of the alveolar space with a granular, pale, eosinophilic material which is positively stained with a PAS reagent. These histological characteristics resemble those of alveolar proteinosis reported in human cases[28,29]. The present result of alveolar proteinosis is consistent with reported findings that a pulmonary administration of ITO to rats and hamsters induces alveolar exudates of proteinaceous materials[8–10]. NTP's study[12] showed that inhalation exposure of rats to indium phosphide aerosol for 14 wk induced accumulation of proteinaceous material within the alveoli, which was diagnosed as alveolar proteinosis. The alveolar proteinosis induced by the inhalation exposures of rats to ITO and IO was similar to that seen in experimental silicosis[30]. Electron-microscopic observation[31] of the lung of rats exposed to pyro-aluminium and quartz showed that pulmonary lesion identical to human alveolar proteinosis is featured by accumulation of PAS-positive alveolar material composed primarily of pulmonary surfactant derived from Type II pneumocytes and large foamy alveolar macrophages with impaired mobility. It is notable that the present finding that the 13-week exposure of rats to 0.1 mg/m^3 ITO induced moderate alveolar proteinosis with a lung content of indium at 24 μg/g lung tissue is comparable with the result of Cummings *et al.*[3], who reported that one of two ITO-exposed workers diagnosed as alveolar proteinosis had 29.3 μg indium per gram of lung tissue. In contrast, occurrence of alveolar proteinosis in workers exposed to ITO has not been definitely demonstrated in any epidemiological studies conducted in Japan[2,4–7]. In particular, Nogami *et al.*[6] reported in their epidemiological study of workers at a Japanese indium plant that neither interstitial nor emphysematous change was recognized in the lung of a worker suffering from bronchioloalveolar carcinoma, while his lung content of indium was 31.2 μg/g lung tissue[6]. These conflicting observations about the occurrence of alveolar proteinosis in indium-exposed workers remain to be resolved, although some etiological factors have been suggested[28–31]. Further experimental toxicology studies will be needed to explore any causative factor of alveolar proteinosis in indium-exposed rodents, including the time- and dose-related changes and species and strain differences.

In the present studies, fibrosis of alveolar wall was found to develop only at the end of 26-week post-exposure period after cessation of the 13-week exposure of rats to ITO at 0.1 mg/m^3. NTP's study[12] also showed that interstitial fibrosis was induced in rats by inhalation exposure to indium phosphide aerosol for 14 wk. The

present finding that 13 wk exposure of rats to ITO induced fibrosis of alveolar wall with the indium burden indicated by 8 μg/g lung and 1 μg/l blood at the end of the 26-week post-exposure period can be contrasted with the case study of Homma *et al.*[32], who showed that an ITO-exposed worker was diagnosed as having pulmonary fibrosis with a serum indium level of 51 μg/l. This apparent difference in the sensitivity to pulmonary fibrosis between rats and humans remains to be resolved and warrants further studies including solubility of ITO in the lung.

ACGIH's recommendation of TLV-TWA[13] for indium and its compounds of 0.1 mg/m^3 was based on pulmonary toxicity of widespread alveolar edema resembling alveolar proteinosis, resulting from 3-month inhalation exposure of rats to IO aerosol[33]. JSOH recommended a BEI of 3 μg/l as a serum level of indium, below which chronic inflammation would not occur[15]. However, it was found in the present studies that both alveolar proteinosis and alveolar macrophage infiltration are induced in rats by 13 wk inhalation exposure to ITO at 0.1 mg/m^3, the same concentration as the ACGIH's TLV-TWA. Moreover, alveolar wall fibrosis and alveolar epithelial hyperplasia develop in all exposed rats at the end of the 26-week post-exposure period, indicating that the persistent fibroproliferative lung lesions develops with a latent period of 26 wk after cessation of the repeated inhalation exposure to 0.1 mg/m^3 ITO. Blood contents of indium are reported to be approximately equal to serum levels of indium[12, 34], while indium levels in blood instead of serum were quantified in the present studies. All the blood levels of indium in the rats exposed to ITO aerosol at 0.1 mg/m^3 measured at the end of the 13-week exposure period and at the end of the 26-week post-exposure period were below the BEI value of 3 μg/l set by JSOH. Therefore, the present findings provide novel information about the animal basis of ITO-induced pulmonary toxicity for reconsideration of the current OEL and BEI for inhaled indium and its compounds.

We consider that an exposure concentration of 0.1 mg/m^3 ITO for 104 wk would be too high for use in a 2-year carcinogenicity study, based on the magnitude of increased lung weights and the increased incidences and severities of pulmonary lesions in the rats exposed to ITO at 0.1 mg/m^3 for 13 wk and for the 26-week post-exposure period after cessation of the 13-week exposure to 0.1 mg/m^3. In the 2-year study, repeated exposure of rats to 0.1 mg/m^3 ITO should be discontinued at the first 26 wk, and then these rats are allowed to continue unexposed in the exposure chamber for the remainder of the study. This exposure discontinuation is based on the 1.7-fold increase in relative lung weight compared with that of the control group, the lack of recovery from alveolar proteinosis, alveolar epithelial hyperplasia, and the development of fibrosis or thickened pleural wall observed at the end of the present study's 26-week post-exposure period, and with reference to NTP's stop-exposure rationale in the 2-year study of indium phosphide carcinogenicity[12]. The middle and lowest exposure concentrations for 104 wk were selected as 0.03 and 0.01 mg/m^3, respectively. The lowest exposure concentration of 0.01 mg/m^3 was set at the lowest concentration that generation of ITO aerosol in the present system and its chamber monitoring of the aerosol can be performed with sufficient reproducibility and accuracy.

Conclusions

Using an aerosol generator and inhalation exposure system with reproducibility and accuracy, rats of both sexes were exposed to ITO and IO at different concentrations for 2 and 13 wk. An exposure concentration-related increase in whole-lung contents of indium tended to be suppressed in the ITO- and IO-exposed rats, and blood contents of indium in the ITO-exposed rats were higher than those in the IO-exposed rats. ITO and IO particles were deposited in the lung, and to a lesser extent in the BALT, MLN and NALT of exposed rats. Two-week exposures to ITO and IO induced alveolar proteinosis, infiltrations of alveolar macrophages and inflammatory cells and alveolar epithelial hyperplasia in addition to increased lung weight. Thirteen-week exposures to ITO and IO induced the similar pulmonary lesions, and some of these lesions were worsened. ITO affected the lung more severely than did IO. Development of fibrosis and worsening of alveolar epithelial hyperplasia were noted at the end of the 26-week post-exposure period following 13 wk exposure. These ITO-induced lesions appeared at the same exposure concentration as ACGIH's TLV and at the blood indium levels below JSOH's BEI.

Acknowledgments: The present studies were contracted with and financially supported by JX Nippon Mining & Metals, Corp. (former Nippon Mining & Metals Co., Ltd.) and other 9 companies. The authors are deeply indebted to all of these companies for allowing us to publish the present studies in a scientific journal for the sake of promotion of occupational health including effective protection of workers from excessive exposure to ITO in the work environment.

References

1) Jorgenson JD, George MW. Mineral Commodity Profile-Indium. Open-File Report 2004-1300. US. Geological Survey, Reston, VA. [Online]. 2005 [cited 2010 Jun 16]; Available from: URL: http://pubs.usgs.gov/of/2004/1300/2004-1300.pdf
2) Homma T, Ueno T, Sekizawa K, Tanaka A, Hirata M. Interstitial pneumonia developed in a worker dealing with particles containing indium-tin oxide. J Occup Health 2003; 45: 137–9.
3) Cummings KJ, Donat WE, Ettensohn DB, Roggli VL, Ingram P, Kreiss K. Pulmonary alveolar proteinosis in workers at an indium processing facility. Am J Respir

Crit Care Med 2010; 181: 458–64.
4) Chonan T, Taguchi O, Omae K. Interstitial pulmonary disorders in indium-processing workers. Eur Respir J 2007; 29: 317–24.
5) Hamaguchi T, Omae K, Takebayashi T, et al. Exposure to hardly soluble indium compounds in ITO production and recycling plants is a new risk for interstitial lung damage. Occup Environ Med 2008; 65: 51–5.
6) Nogami H, Shimoda T, Shoji S, Nishima S. Pulmonary disorders in indium-processing workers. J JPN Respir Soc 2008; 46: 60–4 (in Japanese).
7) Nakano M, Omae K, Tanaka A, et al. Causal relationship between indium compound inhalation and effects on the lungs. J Occup Health 2009; 51: 513–21.
8) Lison D, Laloy J, Corazzari I, et al. Sintered indium-tin-oxide (ITO) particles: a new pneumotoxic entity. Toxicol Sci 2009; 108: 472–81.
9) Tanaka A, Hirata M, Omura M, et al. Pulmonary toxicity of indium-tin oxide and indium phosphide after intratracheal instillations into the lung of hamsters. J Occup Health 2002; 44: 99–102.
10) Tanaka A, Hirata M, Homma T, Kiyohara Y. Chronic pulmonary toxicity study of indium-tin oxide and indium oxide following intratracheal instillations into the lungs of hamsters. J Occup Health 2010; 52: 14–22.
11) Blazka ME, Dixon D, Haskins E, Rosenthal GJ. Pulmonary toxicity to intratracheally administered indium trichloride in Fischer 344 rats. Fundam Appl Toxicol 1994; 22: 231–9.
12) National Toxicology Program (NTP). Toxicology and carcinogenesis studies of indium phosphide (CAS No. 22398-80-7) in F344/N rats and B6C3F$_1$ mice (Inhalation studies). NTP TR 499. Research Triangle Park (NC): U.S. Department of Health and Human Service, Public Health Service, National Institute of Health; 2001.
13) American Conference of Governmental Industrial Hygienists (ACGIH). Indium and compounds. In: Documentation of the threshold limit values (TLVs) and biological exposure indices (BEIs) [CD-ROM 2007]. Cincinnati (OH): ACGIH; 2001.
14) National Institute for Occupational Safety and Health (NIOSH). NIOSH pocket guide to chemical hazards–Indium. [Online]. 2005 [cited 2010 Jun 10]; Available from: URL: http://www.cdc.gov/niosh/npg/npgd0341.html
15) Japan Society for Occupational Health (JSOH). Documentation of OEL and BEI for indium and its compounds. San Ei Shi 2007; 49: 196–202 (in Japanese).
16) Organization for Economic Co-operation and Development (OECD). OECD principles on good laboratory practice. OECD series on principles of good laboratory practice and compliance monitoring No.1. ENV/MC/CHEM (98) 17. Paris (France): OECD; 1998.
17) Organization for Economic Co-operation and Development (OECD). OECD guideline for testing of chemicals. Repeated dose inhalation toxicity: 28-day or 14-day study. Adopted 12 May, 1981. Paris (France): OECD; 1981.
18) Organization for Economic Co-operation and Development (OECD). OECD guideline for testing of chemicals. Subchronic inhalation toxicity: 90-day study. Adopted 12 May, 1981. Paris (France): OECD; 1981.
19) National Research Council (NRC). Guide for the care and use of laboratory animals. Washington, DC: National Academies Press; 1996.
20) Shackelford C, Long G, Wolf J, Okerberg C, Herbert R. Qualitative and quantitative analysis of nonneoplastic lesions in toxicology studies. Toxicol Pathol 2002; 30: 93–6.
21) Aiso S, Arito H, Nishizawa T, Nagano K, Yamamoto S, Matsushima T. Thirteen-week inhalation toxicity of *p*-dichlorobenzene in mice and rats. J Occup Health 2005; 47: 249–60.
22) Kabe I, Omae K, Nakashima H, et al. *In vitro* solubility and *in vivo* toxicity of indium phosphide. J Occup Health 1996; 38: 6–12.
23) Dittmar TB, Fernando Q, Leavitt JA, McIntyre Jr LC. Surface concentrations of indium, phosphorus, and oxygen in indium phosphide single crystals after exposure to Gamble solution. Anal Chem 1992; 64: 2929–33.
24) Brain JD, Curran MA, Donaghey T, Molina RM. Biologic responses to nanomaterials depend on exposure, clearance, and material characteristics. Nanotoxicol 2009; 3: 174–80.
25) Suzuki Y, Matsushita H. Interaction of metal ions with phospholipid monolayer and their acute toxicity. Ind Health 1969; 7: 143–54.
26) Fan JCC, Goodenough JB. X-ray photoemission spectroscopy studies of Sn-doped indium-oxide films. J Appl Phys 1977; 48: 3524–31.
27) Morrow PE. Possible mechanisms to explain dust overloading of the lungs. Fundam Appl Toxicol 1988; 10: 369–84.
28) Rosen SH, Castleman B, Liebow AA, et al. Pulmonary alveolar proteinosis. The New England J Med 1958; 258: 1123–42.
29) Davidson JM, Macleod WM. Pulmonary alveolar proteinosis. Brit J Dis Chest 1969; 63: 13–28.
30) Gross P, deTreville RTP. Alveolar proteinosis. Its experimental production in rodents. Arch Path 1968; 86: 255–61.
31) Corrin B, King E. Pathogenesis of experimental pulmonary alveolar proteinosis. Thorax 1970; 25: 230–6.
32) Homma S, Miyamoto A, Sakamoto S, Kishi K, Motoi N, Yoshimura K. Pulmonary fibrosis in an individual occupationally exposed to inhaled indium-tin oxide. Eur Respir J 2005; 25: 200–4.
33) Leach LJ, Scott JK, Armstrong RD, Steadman LT, Maynard EA. The inhalation toxicity of indium sesquioxide in the rat. The University of Rochester Atomic Energy Project, Report No.UR-590. Rochester (NY): Univ of Rochester; 1961.
34) Miyaki K, Hosoda K, Hirata M, et al. Biological monitoring of indium by means of graphite furnace atomic absorption spectrophotometry in workers exposed to particles of indium compounds. J Occup Health 2003; 45: 228–30.

J Occup Health 2011; 53: 234–239

Journal of Occupational Health

Brief Report

Pulmonary Toxicity in Mice by 2- and 13-week Inhalation Exposures to Indium-tin Oxide and Indium Oxide Aerosols

Kasuke NAGANO[1], Tomoshi NISHIZAWA[1], Yoko EITAKI[2], Makoto OHNISHI[1], Tadashi NOGUCHI[1], Heihachiro ARITO[1] and Shoji FUKUSHIMA[1]

[1]Japan Bioassay Research Center, Japan Industrial Safety and Health Association and [2]Occupational Health Research and Development Center, Japan Industrial Safety and Health Association, Japan

Abstract: Pulmonary Toxicity in Mice by 2- and 13-week Inhalation Exposures to Indium-tin Oxide and Indium Oxide Aerosols: Kasuke NAGANO, *et al.*, Japan Bioassay Research Center, Japan Industrial Safety and Health Association—Objectives: Inhalation toxicities of indium-tin oxide (ITO) and indium oxide (IO) in mice were characterized in comparison with those previously reported in rats. **Methods:** B6C3F$_1$ mice of both sexes were exposed by inhalation to ITO or IO aerosol for 6 h/day, 5 day/wk for 2 wk at 0, 0.1, 1, 10 or 100 mg/m^3 or 13 wk at 0, 0.1or 1 mg/m^3. **Results:** ITO and IO particles were deposited in the lung, mediastinal lymph node (MLN) and nasal-associated lymphoid tissue. Alveolar proteinosis, infiltrations of alveolar macrophages and inflammatory cells and increased lung weight were induced by 2- and 13-week exposures to ITO and IO, while alveolar epithelial hyperplasia occurred only in the 2-week exposures. Thickened pleural wall, hyperplastic MLN, extramedullary hematopoiesis in the spleen and increased levels of erythrocyte parameters were induced by 13-week exposure to ITO. The ITO- and IO-induced pulmonary lesions were milder in mice than those previously reported in rats, and the fibrotic lesions were different between these two species. Indium levels in the lung and pooled blood were analyzed in the mice exposed to ITO and IO for 13 wk. In the 13-week inhalation exposure of mice to ITO, alveolar proteinosis and significantly increased lung weight were induced at the same exposure concentration as the current threshold limit value for indium and its compounds.
(J Occup Health 2011; 53: 234–239)

Received Dec 2, 2010; Accepted Jan 25, 2011
Published online in J-STAGE Mar 16, 2011
Correspondence to: T. Nishizawa, Japan Bioassay Research Center, Japan Industrial Safety and Health Association, 2445 Hirasawa, Hadano, Kanagawa 257-0015, Japan
(e-mail: t-nishizawa@jisha.or.jp)

Key words: Indium oxide, Indium-tin oxide, Inhalation, Lung, Mouse, Toxicity

Serious concerns have been raised over workers' health in the plants where indium-tin oxide (ITO) is manufactured and processed. Fatal case studies[1, 2] and epidemiology studies of workers[3–6] have demonstrated that inhalation of indium is a potential cause of occupational lung disease and increases the risk of interstitial lung damage. Experimental toxicology studies have shown that an intratracheal administration of ITO powder induces persistent inflammation in the lung without any significant fibrotic response in rats[7], and elicits pulmonary inflammatory response with diffuse alveolar or bronchiolar cell hyperplasia and interstitial fibrotic proliferation in hamsters[8, 9]. Our previous study[10] showed that 2- and 13-week inhalation exposures of rats to ITO or indium oxide (IO) aerosol induce pulmonary fibrosis, alveolar proteinosis and macrophage infiltration.

The present studies were intended to characterize inhalation toxicities of ITO and IO aerosols in mice in comparison with those reported in rats[10].

Materials and Methods

The present studies were performed with the approval of the ethics committee of the Japan Bioassay Research Center. The animals were cared for in accordance with a guide for the care and use of laboratory animals. All these related documentations were cited in our previous rat studies[10].

ITO and IO powders were the same as those used in our previous rat studies[10], which were kindly supplied by JX Nippon Mining & Metals, Corp (Tokyo, Japan).

B6C3F$_1$/Crlj mice of both sexes were obtained at the age of 4 wk from Charles River Japan, Inc (Kanagawa, Japan). The animals were quarantined and acclimated for 2 wk before the start of experiment. The mice were individually housed in stainless-steel wire hanging cages

(112 W × 212 D × 120 H mm), and placed in stainless steel inhalation exposure chambers. Environment in the exposure chamber, lighting, and supply of food and drinking water were maintained under the same conditions as described in our previous rat study[10].

In the 2-week study, groups of 5 mice of both sexes were exposed to ITO or IO aerosol at a target concentration of 0.1, 1, 10 or 100 mg/m^3 for 6 h/day, 5 day/wk for 2 wk. In the 13-week study, groups of 10 mice of both sexes were exposed to ITO or IO aerosol at a target concentration of 0.1 or 1 mg/m^3 for 6 h/day, 5 day/wk for 13 wk. Groups of 5 or 10 mice of both sexes were exposed to clean air for 2 or 13 wk, and served as respective controls.

The aerosol generation and exposure system and the methods for measurements of the exposure concentrations and size distributions of ITO and IO aerosols, and for clinical and pathological examinations and analysis of indium in the lung and blood as well as statistical analysis were the same as those described in our previous rat study[10].

Results

Chamber concentrations and size distributions of ITO and IO aerosols

Chamber concentrations of ITO and IO aerosols were controlled precisely within less than 10% in the variation coefficient and accurately within less than 10% deviation from the target concentrations. Mass median aerodynamic diameters (MMADs) of ITO aerosol in the exposure chamber ranged from 2.4 to 3.8 μm in the 2-week study, and from 2.3 to 2.6 μm in the 13-week study, and geometric standard deviations (GSDs) ranged from 1.6 to 2.4. MMADs of IO aerosol ranged from 1.9 to 2.3 μm, and GSDs ranged from 1.5 to 2.1.

Mortality and clinical signs, and hematology

Neither death, abnormal clinical sign nor growth retardation occurred in any group exposed to ITO, IO or clean air for 2 or 13 wk. In the 13-week study, red blood cell counts, hemoglobin concentration and hematocrit value were significantly increased in the 0.1 and 1 mg/m^3 ITO-exposed groups compared with the respective controls (data not shown). However, 13-week exposure to IO did not induce any hematological changes.

Lung and spleen weights

In the 2-week study (Table 1), the relative lung weights were significantly increased in the 1 mg/m^3 ITO-exposed female mice and in the 10 and 100 mg/m^3 ITO- and IO-exposed mice of both sexes compared with the respective controls. In the 13-week study (Table 2), the relative lung weights in the 0.1 and 1 mg/m^3 ITO-exposed mice of both sexes and in the 1 mg/m^3 IO-exposed mice of both sexes were significantly increased compared with the respective controls. The relative spleen weight was significantly increased in the 1 mg/m^3 ITO- and IO-exposed mice of both sexes in the 13-week study compared with the respective control.

Histopathological findings

In the 2-week study, ITO and IO particles were deposited separately as single particles in the lungs of almost all 1, 10 and 100 mg/m^3 ITO- and IO-exposed mice (Table 1). The particles of ITO and IO were pale brown and transparent, looked like amber, and were located primarily within alveolar macrophages. ITO and IO particles were also deposited in the mediastinal lymph node (MLN) of the 10 and 100 mg/m^3 ITO- and IO-exposed mice, and in the nasal-associated lymphoid tissue (NALT) of the nasopharyngeal duct of a few 10 and 100 mg/m^3 IO-exposed male mice. The most remarkable lung lesion found in the 2-week study was alveolar proteinosis, characterized by filling of the alveolar space with a granular, pale eosinophilic material, which was positively stained with a PAS reagent. This lesion was found in all the 10 and 100 mg/m^3 ITO- and IO-exposed mice. The severity score of alveolar proteinosis was higher in the 100 mg/m^3 ITO-exposed mice of both sexes than in the 100 mg/m^3 IO-exposed mice. Hyperplasia of alveolar epithelium and infiltration of inflammatory cells composed of neutrophils and lymphocytes were observed primarily in the 100 mg/m^3 ITO- and IO-exposed mice. Hyperplasia of the alveolar epithelium was characterized by the increased numbers of cuboidal cells which were assumed to be type II pneumocytes. Infiltration of alveolar macrophages was found in a few 100 mg/m^3 ITO-exposed mice and in one 100 mg/m^3 IO-exposed male mouse.

In the 13-week study, ITO and IO particles were deposited separately as single particles in the lungs of all the 0.1 and 1 mg/m^3 ITO- and IO-exposed mice (Table 2). Those particles were also deposited in the MLN of the 0.1 and 1 mg/m^3 ITO-exposed mice and the 1 mg/m^3 IO-exposed mice. Significantly increased incidences of alveolar proteinosis in the 0.1 and 1 mg/m^3 ITO-exposed mice and in the 1 mg/m^3 IO-exposed mice and infiltrations of alveolar macrophages and inflammatory cells in the 1 mg/m^3 ITO- and IO-exposed mice were noted. Swelling of cytoplasm was recognized in the alveolar macrophages engulfing the particles. Alveolar wall fibrosis was not found in any mouse exposed to either ITO or IO. Thickening of pleural wall and hyperplasia of the MLN occurred in the 1 mg/m^3 ITO-exposed mice. The thickened pleural wall was characterized by an increase in collagen-like connective tissue in the interstitium, and was located in focal lung areas. However, ITO particles were not found in the area of the thickened pleural wall. Hyperplasia of the MLN was characterized by increased numbers of lymphocytes resulting in increased MLN size and area of lymphoid follicles. Extramedullary hematopoiesis occurred in the red pulp of the spleen of the 1 mg/m^3 ITO-